New BIOTECHNOLOGY 95 (2026) 113–127

Contents lists available at ScienceDirect

New BIOTECHNOLOGY

journal homepage: www.elsevier.com/locate/nbt

Alcohol oxidase-free methanol assimilation boosts carbon efficiency and product yield in industrial yeasts

Charles Moritz [a,b], Verena Enzinger [a,b], Viktoria Kowarz [a], Manja Mølgaard Severinsen [a], Lisa Lutz [a,b], Michael Baumschabl [a,b], Daniel Ahlheit [a], Benjamin L. Coltman [a], Luca Hodes [c], Jean-Marc Daran [c], Özge Ata [a,b,*], Diethard Mattanovich [a,b]

[a] BOKU University, Institute of Microbiology and Microbial Biotechnology, Department of Biotechnology and Food Science, Vienna, Austria
[b] Austrian Centre of Industrial Biotechnology (ACIB), Vienna, Austria
[c] Department of Biotechnology, Delft Technical University, Delft, the Netherlands

ARTICLE INFO

Keywords:
Methylotrophy
Energy conservation
Yeast
Synthetic biology
Carbon efficiency
Adaptive laboratory evolution
Flux coupling
Bioeconomy

ABSTRACT

Methanol is an attractive single-carbon feedstock for scalable bioprocesses that avoids the consumption of agricultural products. Native yeast methylotrophy relies on alcohol oxidase (Aox), which dissipates reducing power and limits carbon conversion efficiency. Here, we replace Aox with the native, NAD^+-dependent alcohol dehydrogenase 2 and eliminate the methanol dissimilatory branch by deleting formaldehyde dehydrogenase (Fld) in the yeasts *Komagataella phaffii* and *Ogataea parapolymorpha*. Engineered strains of both species sustain methylotrophic growth despite each modification being individually growth-defective. *FLD* deletion eliminates competition for cytosolically produced formaldehyde and enforces flux coupling between methanol utilization and NADH formation. Adaptive laboratory evolution over 30–50 generations yielded growth rates comparable to industrial yeast strains. In methanol-limited chemostats, evolved Adh-Δfld strains reduced specific CO_2 production 2-fold while increasing biomass yield 1.4-fold. The biomass-per-methanol yields of 0.48 g g^{-1} for *K. phaffii* and 0.43 g g^{-1} for *O. parapolymorpha* are the highest reported for each species. The Adh-based metabolic framework also enabled gram-per-liter itaconic acid production with higher product yield and lower CO_2 evolution than Aox-based strains, underscoring its utility for growth-coupled bioproduction. Adh-coupled methanol oxidation represents a generalizable strategy to increase carbon efficiency in other C1 utilization pathways and yeast species, providing a foundation for more sustainable biomanufacturing processes with yeasts.

1. Introduction

Microorganisms across all three domains of life have evolved the ability to utilize methanol as a carbon and energy source. These organisms, collectively termed methylotrophs, are commonly found on aerial plant surfaces, soil, compost, and in lake sediment environments, where methanol is released through plant pectin degradation [1]. Beginning in the 1970s-1980s, methylotrophic yeasts and bacteria isolated from such environments were exploited for large-scale production of single cell protein (SCP) from petrochemically-sourced methanol [2–4]. In recent years, with increased awareness of the dual challenges of CO_2 emissions and land-use change, there has been a returned focus on methanol as a feedstock for microbial conversion [5]. Green methanol, produced from CO_2 and renewable hydrogen, represents a promising carbon-negative, energy-dense, liquid feedstock, that is already being deployed at industrial-scale [6,7]. Importantly, methanol production can be decoupled from arable land use, avoiding the indirect land-use change and deforestation associated with glucose-based microbial processes [8,9]. The conversion of methanol into bulk chemicals such as organic acids offers a pathway toward replacing petrochemical feedstocks in industrial polymers, lubricants, and adhesives [10–13]. Yeast SCP is already widely used in the agricultural industry and can be considered a valuable primary or side product [14]. In these contexts, maximizing conversion efficiency is essential to minimize life-cycle emissions and ensure economic feasibility of large-volume bioprocesses to minimize the carbon footprint and make economics feasible

* Corresponding author at: BOKU University, Institute of Microbiology and Microbial Biotechnology, Department of Biotechnology and Food Science, Vienna, Austria.
E-mail address: oezge.ata@boku.ac.at (Ö. Ata).

https://doi.org/10.1016/j.nbt.2026.08.006
Received 11 May 2026; Received in revised form 10 August 2026; Accepted 17 August 2026
Available online 18 August 2026

[15,16].

Methanol metabolism in methylotrophic yeasts and bacteria shares a common architecture: methanol is oxidized to formaldehyde, which is either assimilated into biomass or further oxidized to generate reducing equivalents. However, bacterial systems generally achieve higher carbon efficiency. This advantage arises from both the methanol oxidation step—mediated by methanol dehydrogenase (Mdh) rather than alcohol oxidase (Aox)—and the use of the ribulose monophosphate (RuMP) cycle instead of the xylulose monophosphate (XuMP) cycle found in yeasts [7]. Gram-negative bacteria typically employ pyrroloquinoline quinone (PQQ)-dependent Mdhs, whereas Gram-positive methylotrophs utilize NAD-dependent Mdhs. Although NAD-dependent Mdhs offer superior energy conservation, their thermodynamic constraints at mesophilic temperatures restrict activity [17], explaining why organisms such as *Bacillus methanolicus* are thermophilic and grow optimally at 50–55 °C [18]. In contrast, PQQ-dependent Mdhs exhibit higher activity under mesophilic conditions, consistent with the ecological niche of many plant-associated methylotrophs such as *Methylobacterium extorquens* [19].

All characterized methylotrophic yeasts rely on alcohol oxidase for methanol oxidation [20,21]. Although Aox-mediated oxidation is less energy efficient than NAD-dependent dehydrogenase reactions, it is thermodynamically favorable at mesophilic temperatures [22]. Yeasts mitigate the toxicity of hydrogen peroxide generated by Aox through compartmentalization within peroxisomes where catalase degrades H_2O_2 [23]. Accordingly, both Aox and XuMP pathway enzymes localize to the peroxisome during growth on methanol in species such as *Komagataella phaffii* (Syn. *Pichia pastoris*) and *Ogataea parapolymorpha* (formerly included in *Hansenula polymorpha*) [24–26]. These yeasts are established industrial platforms for heterologous protein production [27–30]. Additionally, both *K. phaffii* and methylotrophic yeasts of the *H. polymorpha* complex, such as *Ogataea polymorpha*, have been engineered for production of a range of organic acids from methanol [31–36]. While *K. phaffii* benefits from advanced strain engineering tools and genome-scale metabolic models [37–40], *O. parapolymorpha* has advantages in certain contexts due to its faster growth rate and thermotolerance [41,42].

Recent work identified that *K. phaffii* possesses a native alcohol dehydrogenase, Adh2, capable of oxidizing methanol in strains lacking alcohol oxidases (Mut$^-$ strains) [43,44]. While no growth phenotype was achieved, these results pointed to the possibility of alcohol oxidase-free methanol utilization in yeasts. Because Adh2 is NAD^+-dependent, methanol oxidation via Adh2 conserves reducing equivalents as NADH, offering improved theoretical energy efficiency compared to Aox-based oxidation [45]. More recently, Adh2 was shown to sustain methanol dissimilation and energy supply in Mut$^-$ synthetic autotrophic *K. phaffii* strains, in which carbon assimilation was provided by an engineered Calvin–Benson–Bassham cycle [46]. These Adh-based strains displayed improved carbon efficiency and enhanced organic acid productivity. However, methanol oxidation in this system served only the dissimilatory branch, as biomass carbon was derived from CO_2. Whether Adh2 can support fully methylotrophic growth—where methanol must supply both energy and biomass carbon—remains unresolved.

Here, we demonstrate that deletion of formaldehyde dehydrogenase (*FLD1*) combined with targeted overexpression of native genes enables Adh2-based (K.p.Mut$^-$fld::Adh) growth of *K. phaffii* on methanol. We extend this strategy to *O. parapolymorpha*, yielding O.p.Mut$^-$fld::Adh strains with faster growth at elevated temperatures. Adaptive laboratory evolution further improves growth in both species, with genome sequencing revealing selective pressure on pathways affecting peroxisomal import, consistent with a role in enabling Adh-based methylotrophy. Chemostat and fed-batch experiments demonstrate improved carbon efficiency for both growth and organic acid production in the engineered strains relative to their Aox-based counterparts. Together, these findings establish Adh-based methanol utilization as a viable strategy to enhance the sustainability and economic performance of methanol-based yeast bioprocesses.

2. Results

2.1. Adh-mediated methanol utilization is feasible and increases theoretical efficiency

Previously engineered strains of *K. phaffii* (CBS2612) were used as a starting point for this work (Table 1) [44]. In these strains, both alcohol oxidases (*AOX1* and *AOX2*) were deleted, generating the Mut$^-$ phenotype, and the native *ADH2* gene was overexpressed in the cytosol (without a peroxisomal targeting sequence) under control of the *AOX1* promoter (Mut$^-$AdhOE). Although neither strain was able to grow on methanol, Mut$^-$AdhOE displayed an elevated methanol uptake rate (q_{MeOH}) compared to the Mut$^-$ strain. ^{13}C-labelling analysis revealed that, while minor methanol assimilation occurred, the majority of carbon flux was directed toward dissimilation to CO_2. We hypothesized that the inability to sustain growth resulted from rapid cytosolic dissimilation of formaldehyde, which is generated by Adh2 outside the peroxisome (Supplementary Fig. S1A). To test this hypothesis, we sought to eliminate the dissimilatory branch, thereby permitting formaldehyde accumulation and diffusion into the peroxisome for assimilation via the XuMP cycle (Fig. 1A,B).

In contrast to Aox-mediated oxidation, Adh2 catalyzes NAD^+-dependent methanol oxidation, generating one cytosolic NADH per methanol. While reported assimilation fractions in *K. phaffii* WT typically range from 50% to 70% [44,47], we assumed a 50:50 assimilation-to-dissimilation split ratio for simplicity to illustrate the relative energetic differences between the WT and Mut$^-$Adh strains (Fig. 1 A,B). Under this assumption, both pathways generate 1 cytosolic NADH per assimilated methanol. While the WT loses a second methanol molecule for dissimilation to CO_2, combining the Mut$^-$Adh pathway with

Table 1
K. phaffii and O. parapolymorpha strains used in this study.

Short name	Genotype	reference
K.p. WT	*K. phaffii* CBS2612	
K.p.Mut$^-$	*K. phaffii* CBS2612 + *aox1*Δ + *aox2*Δ	Zavec et al. (2021).
K.p. Mut$^-$AdhOE	*K. phaffii* CBS2612 + *aox1*Δ + *aox2*Δ + aZ_pAOX1_*ADH2*	Zavec et al. (2021).
CBS7435 ΔFLD	*K. phaffii* CBS2612 + *fld1*Δ (CRISPR)	This study
CBS2612 ΔFLD	*K. phaffii* CBS2612 + *fld1*Δ:mcherry (split marker)	This study
K.p.Mut$^-$fld::Adh_cr	K.p.Mut$^-$AdhOE + *fld1*Δ::*ADH2* (CRISPR)	This study
K.p.Mut$^-$fld::Adh_sm	K.p.Mut$^-$AdhOE + *fld1*Δ:: pDAS2_*DAS2*_pAOX_*ADH2* (split marker)	This study
K.p.ALE1.1	K.p.Mut$^-$fld::Adh_cr + ALE (30 generations) Population 1, clone 1	This study
K.p.ALE1.2	K.p.Mut$^-$fld::Adh_cr + ALE (30 generations) Population 2, clone 3	This study
K.p.ALE2.1	K.p.Mut$^-$fld::Adh_sm + ALE (30 generations) Population 1, clone 1	This study
K.p.ALE2.2	K.p.Mut$^-$fld::Adh_sm + ALE (30 generations) Population 2, clone 2	This study
O.p. WT	*O. parapolymorpha* DL1	This study
O.p. Mut$^-$AdhOE	*O. parapolymorpha* DL1 + *aox*Δ::*ADH2*	This study
O.p.Mut$^-$fld::Adh	O.p.Mut$^-$AdhOE + *fld*Δ:: pDAS_DAS_pAOX_*ADH2*	This study
O.p.ALE.1	O.p.Mut$^-$fld::Adh + ALE (50 generations) Population 1, clone 2	This study
O.p.ALE.2	O.p.Mut$^-$fld::Adh + ALE (50 generations) Population 2, clone 1	This study
ITA	*K. phaffii* CBS7435 pAOX1_*cadA* + pPOR1_*mttA* + pGAP_*mfsA*	Severinsen et al. (2024)
ITA-Mut^S	ITA + *aox1*Δ	This study
ITA-Mut$^-$fld::Adh	ITA + *aox2*Δ + *aox1*Δ::Adh2 + *fld*Δ (CRISPR)	This study

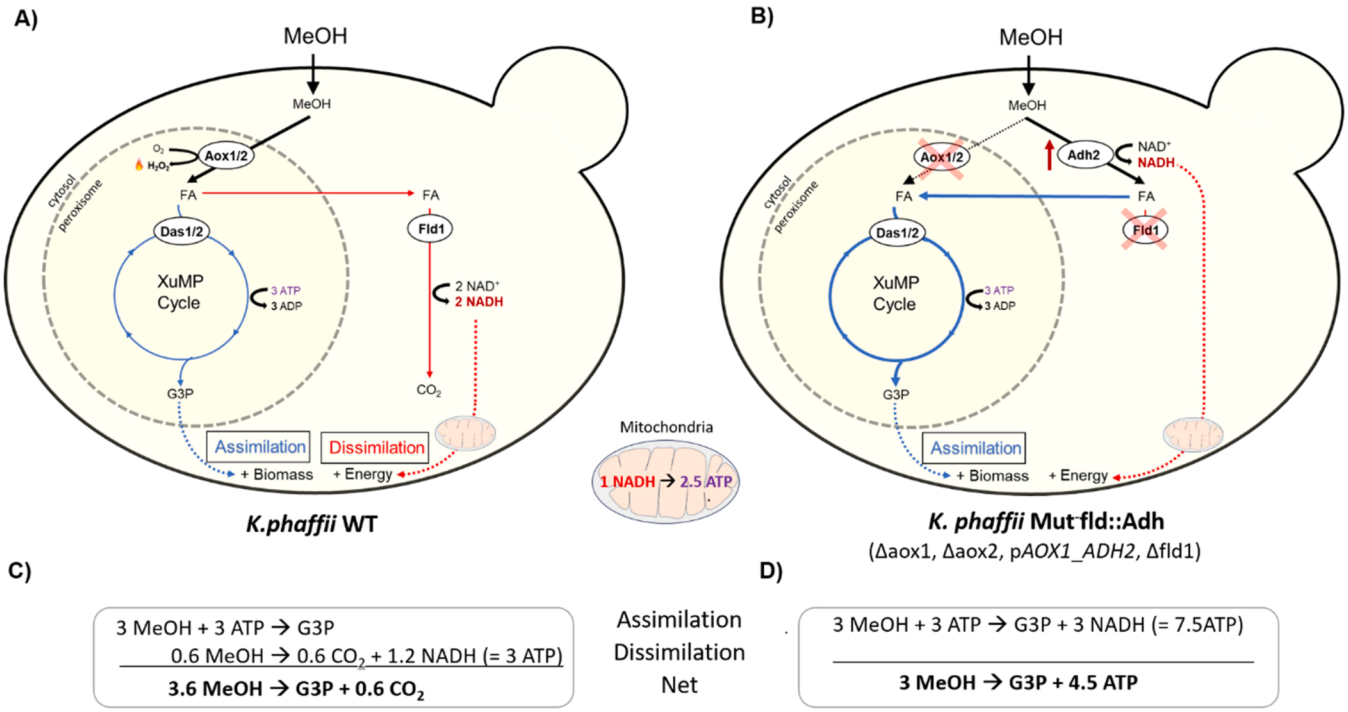

Fig. 1. Comparison of methanol metabolism of *K. phaffii* wild type and engineered Mut⁻fld::Adh strains A) In the wild type (WT) methanol is oxidized in the peroxisome by alcohol oxidases (Aox1/2), producing formaldehyde (FA) and hydrogen peroxide (H_2O_2) in a highly exothermic reaction. Formaldehyde then either enters the assimilatory pathway or diffuses to the cytosol where it is dissimilated to CO_2, producing 2 NADH. B) Metabolic engineering strategy to achieve growth in Mut⁻Adh *K. phaffii* strain. The dissimilatory pathway is removed by deletion of formaldehyde dehydrogenase (Fld1). Formaldehyde produced by the Adh2 reaction may then diffuse readily into the peroxisome for assimilation. Cytosolic NADH is produced through the Adh2 reaction instead of the CO_2-producing dissimilatory pathway. C) Stoichiometric calculations for conversion of methanol to glyceraldehyde 3-phosphate (G3P) in wild type *K. phaffii*. 3 ATP is required to produce one G3P from 3 methanol via the XuMP pathway. To meet this energy demand, 0.6 methanol must be dissimilated to produce 1.2 NADH (equivalent to 3 ATP), releasing 0.6 CO_2. D) Stoichiometric calculations for conversion of methanol to G3P in engineered Mut⁻fld::Adh strains. The oxidation of 3 MeOH by Adh2 produces 3 NADH (7.5 ATP), which provides energy in excess of requirements of the assimilatory branch. No CO_2 must be produced to satisfy the conversion of methanol to G3P, and 4.5 net ATP are produced. Excess energy produced can serve to satisfy maintenance energy demands of the cell. A conversion of 1 NADH to 2.5 ATP was used based on the malate aspartate shuttle being used to transfer electrons from the cytosolically produced NADH to the electron transfer chain. Aox1/2, alcohol oxidase; Adh2, alcohol dehydrogenase 2; Das1/2, dihydroxyacetone synthase; MeOH, methanol; FA, formaldehyde; G3P, glyceraldehyde 3-phosphate; XuMP cycle, xylulose monophosphate cycle.

a deletion of the dissimilatory pathway would avoid the loss of carbon while maintaining the generation of reducing power. In contrast, Adh2-based methanol oxidation in the non-growing strain K.p. Mut-AdhOE would generate on average 2 NADH per methanol utilized, potentially imposing an additional limitation on growth due to an imbalance in cellular reducing power (Supplementary Fig. S1A). Thus, removal of the dissimilatory pathway from the strain K.p.Mut⁻AdhOE (yielding strain Mut⁻fld::Adh) was predicted to restore redox balance while directly coupling methanol oxidation and energy generation to biomass growth and product formation [48].

Stoichiometric calculations for methanol assimilation to glyceraldehyde3-phosphate (G3P) in the wild type indicate that approximately 0.6 mol methanol must be oxidized to CO_2 to provide sufficient energy for assimilation (Fig. 1 C). In contrast, the Mut⁻fld::Adh configuration theoretically eliminates this CO_2 release and yields a surplus of 4.5 ATP equivalents per G3P produced (Fig. 1D). This additional ATP can partially offset maintenance energy demands, thereby reducing theoretical CO_2 evolution (q_{CO_2}) and increasing the predicted biomass yield ($Y_{X/S}$).

Genome-scale metabolic modelling was performed to assess the feasibility of the proposed strains and to obtain process-relevant predictions of carbon efficiency improvements. Deletions of *AOX1*, *AOX2*, and *FLD1* were implemented in the iMT1026v3 model [40] by setting the flux through the reactions to zero, and a cytosolic Adh2-catalyzed methanol oxidation reaction was added. Flux balance analysis (FBA) simulations predicted an approximately 50% increase in the maximum theoretical biomass yield of the K.p.Mut-fld::Adh strain compared with the WT (0.405 vs. 0.602 g g^{-1}) (Fig. 2 A). The resulting biomass yield curves are asymptotic because non-growth-associated maintenance energy (NGAME) constitutes a relatively large fraction of methanol consumption at low growth rates. As the growth rate increases, biomass formation becomes the dominant methanol requirement, and the predicted yield approaches its theoretical maximum. Simulated physiological parameters across a range of growth rates (0.02 h^{-1} - 0.2 h^{-1}) are provided in Supplementary Table S1.

To further validate the feasibility of Adh2-based methanol utilization in *K. phaffii*, native Adh2 was isolated and characterized in vitro. An N-terminally His-tagged Adh2 was purified by immobilized metal affinity chromatography, and its kinetic parameters and temperature dependence were determined (Fig. 2B,C). Consistent with improved thermodynamic favorability at elevated temperatures, Adh2 activity increased between 30 °C and 40 °C. Both k_{cat} and K_m improved at 40 °C, resulting in a 2.2-fold increase in catalytic efficiency (k_{cat}/K_m) under saturating NAD^+ conditions, demonstrating enhanced enzyme performance at higher temperature (Supplementary Table S2).

2.2. Adh-based growth on methanol is achieved in Komagataella phaffii and Ogataea parapolymorpha through removal of the dissimilatory pathway

As was also found by Zavec et al., the K.p.Mut⁻AdhOE strain could not grow on methanol (Fig. 3A) [44]. Similarly, when *FLD1* was knocked

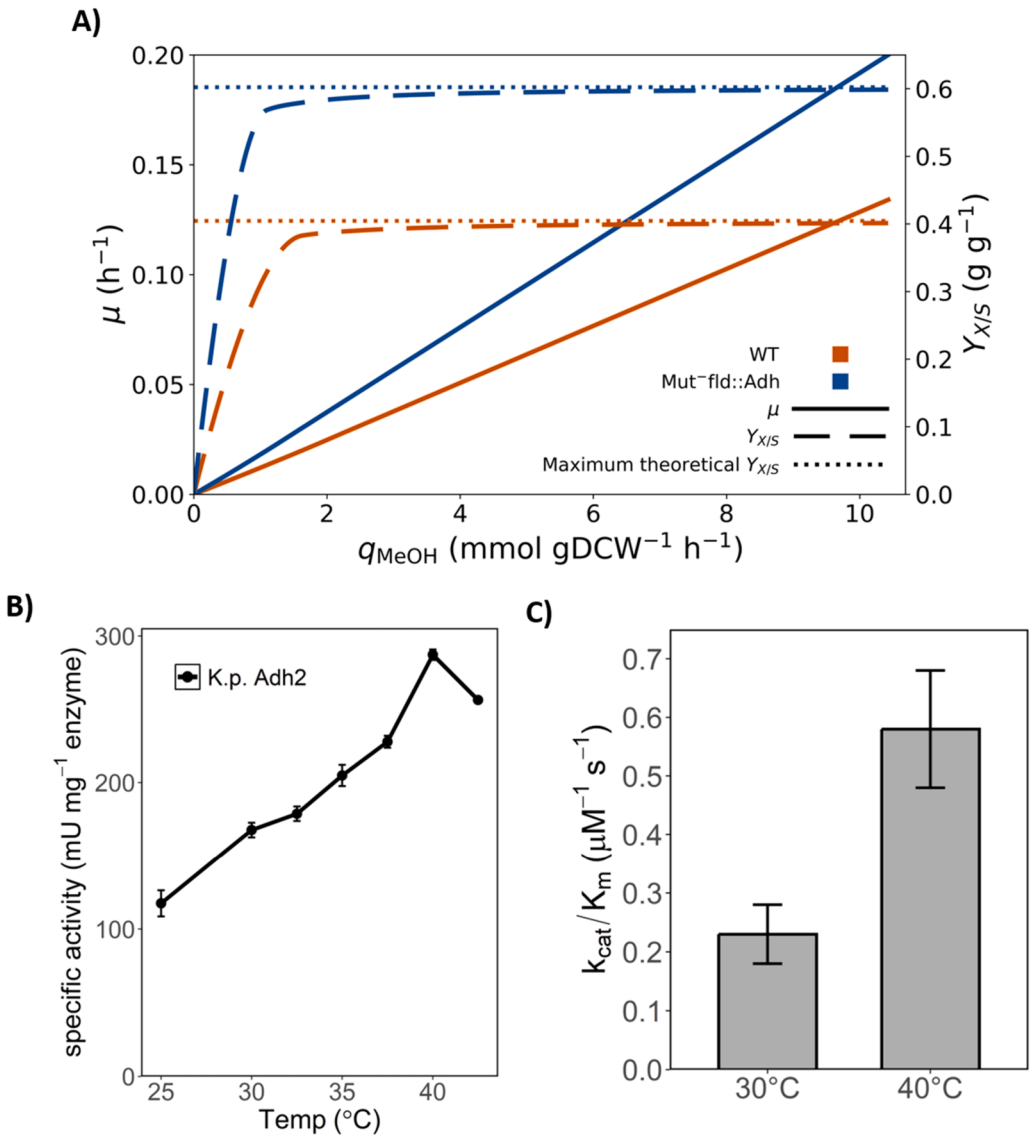

Fig. 2. Genome-scale metabolic modelling and in vitro kinetic characterization of *K. phaffii* alcohol dehydrogenase 2 (Adh2). A) Predicted specific methanol uptake rate (q_{MeOH}) in relation to the specific growth rate (μ) and biomass yield (g g^{-1} methanol) for Mut^+ (WT) (orange) and engineered K.p.Mut⁻fld::Adh (*aox1*Δ, *aox2*Δ, *fld1*Δ) (blue). Please see the Methods section for details of the modelling approach and the accompanying Supplementary Python script. B) In vitro determination of the temperature dependence of *K. phaffii* (K.p.) Adh2 activity toward methanol. Error bars indicate standard deviation (SD) calculated from triplicate measurements (n = 3). C) Catalytic efficiency (k_{cat}/K_m) of K.p. Adh2 measured at two temperatures at pH7.5. Error bars represent standard errors (SE) derived from Hanes–Woolf regression with error propagation from duplicate measurements. Additional data on Adh2 purification and kinetic characterization are provided in Supplementary Table S2.

out in wild-type CBS2612 and CBS7435, both strains were unable grow (Supplementary Fig. S3). Following our hypothesis outlined in the previous section, the *FLD1* gene was knocked out in the strain K.p.Mut⁻AdhOE using CRISPR-Cas9 editing (K.p.Mut⁻fld::Adh_cr). This strain, which was a combination of two non-growing phenotypes, was able to grow on methanol with maximum specific growth rate (μ_{max}) of 0.0130 ± 0.0008 h^{-1} and an overall specific growth rate ($\mu_{overall}$) of 0.0065 ± 0.0002 h^{-1} over the course of the cultivation (Fig. 3 A). In hopes of generating a strain with faster growth, an additional K.p.Mut⁻fld::Adh strain was constructed by integrating overexpression cassettes of *DAS2* and *ADH2* within the *FLD1* gene (K.p.Mut⁻fld::Adh_sm). This strain also grew on methanol, although at a slightly reduced rate (μ_{max} = 0.0123 ± 0.0006 h^{-1}, $\mu_{overall}$ = 0.0061 ± 0.0003 h^{-1}) compared with K.p. Mut⁻fld::Adh_cr (Fig. 3 A).

NAD^+-dependent methanol oxidation is predicted to exhibit greater thermodynamic favorability at elevated temperatures [22]. Consistent with this, methylotrophic bacteria that utilize methanol dehydrogenases typically grow at 40–60 °C, with optima between 50–55 °C [49]. Supported by our in vitro Adh2 kinetic data, we hypothesized that increasing cultivation temperature could enhance Adh-mediated flux and thereby improve growth of Adh-based strains. However, *K. phaffii* exhibits optimal growth at 28–30 °C, with growth rates declining rapidly at higher temperatures [50]. We therefore explored elevated-temperature Adh-based growth in the related methylotrophic yeast *O. parapolymorpha*. This species has been reported to grow on methanol at temperatures up to 50 °C and exhibits an optimal growth temperature of approximately 40 °C [28], coinciding with the temperature optimum observed for *K. phaffii* Adh2 (Fig. 2B,C). Methanol metabolism in *O. parapolymorpha* DL1 closely resembles that of *K. phaffii*, including peroxisomal Aox-mediated methanol oxidation, peroxisomal localization of the XuMP pathway enzymes, and cytosolic formaldehyde dissimilation to CO_2 [51]. Genome annotation indicates a single copy of alcohol oxidase (*AOX*, HPODL_03886) and dihydroxyacetone synthase (*DAS*, HPODL_04602), as well as two *ADH2* homologs

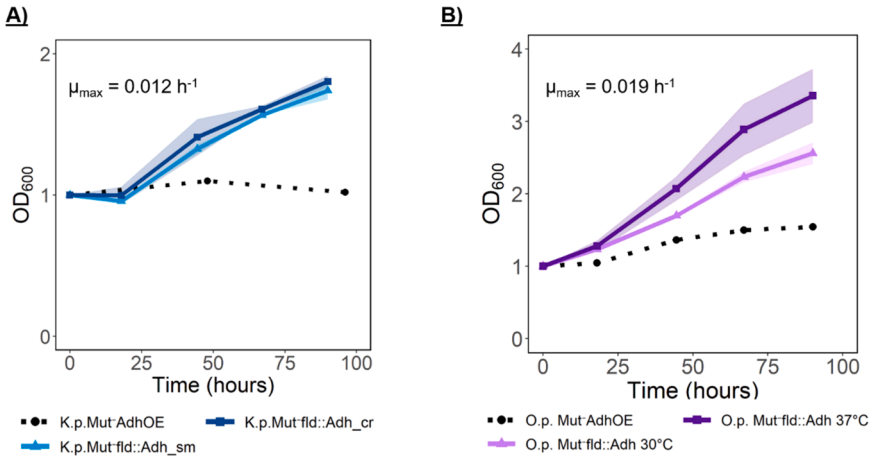

Fig. 3. Shake flask cultivations of engineered Adh-based strains on minimal methanol media (YNB). A) Growth of parental strain *K. phaffii* (K.p.) Mut⁻AdhOE compared with K.p.Mut⁻fld::Adh_cr and K.p.Mut⁻fld::Adh_sm, B) Growth of parental strain *O. parapolymorpha* (O.p.) Mut⁻AdhOE at 37°C compared with O.p.Mut⁻fld::Adh at both 30°C and 37°C. In both panels, OD_{600} values were normalized to the initial OD_{600} at the start of the cultivation. Error shading represent the standard deviations from the means for two biological replicates. K.p.Mut-AdhOE was cultivated in a separate experiment under identical conditions, and the data shown represent the mean of technical replicates. The μ_{max} values shown in panels A and B correspond to the K.p.Mut-fld::Adh_cr and O.p.Mut-fld::Adh clones, respectively, selected for the subsequent adaptive laboratory evolution (ALE) experiment and were calculated from the OD_{600} measurements between 18 and 45 h.

(HPODL_02528 and HPODL_03666). Sequence analysis revealed a predicted mitochondrial targeting sequence in HPODL_02528, which we therefore designated *ADH3*, while HPODL_03666 was considered the cytosolic *ADH2* ortholog. Using the CRISPR-Cas9 system developed for *K. phaffii* [39], we engineered Adh-based methanol utilization in *O. parapolymorpha*. To enhance recombination efficiency, 1000 bp homology arms flanking the targeted cut sites were employed instead of the conventional 250–500 bp regions. The native *AOX* coding sequence was replaced with the endogenous *O. parapolymorpha ADH2* to generate strain O.p.Mut⁻AdhOE. Subsequently, *FLD* (*FLD1* ortholog) was disrupted by insertion of *DAS* (*DAS1/2* ortholog) within the coding sequence, yielding strain O.p.Mut⁻fld::Adh. As observed in *K. phaffii*, deletion of *AOX* in *O. parapolymorpha* abolished growth on methanol (Fig. 3B). Subsequent disruption of *FLD* then restored the growth phenotype, consistent with the results obtained in *K. phaffii*. The maximum specific growth rate (μ_{max}) of O.p.Mut⁻fld::Adh reached 0.018 ± 0.001 h^{-1} at 37 °C compared to 0.012 ± 0.001 h^{-1} for the same strain at 30 °C. Beyond higher thermotolerance and faster growth, these results further support the conclusion that Adh-mediated methanol oxidation can sustain methylotrophic growth in yeasts when cytosolic formaldehyde dissimilation is eliminated.

2.3. Adaptive laboratory evolution enhances growth of Mut⁻fld::Adh strains

Once a sustained growth phenotype was achieved, we then improved the growth rate of both *K. phaffii* and *O. parapolymorpha* Mut⁻fld::Adh strains through adaptive laboratory evolution (ALE) [52,53]. Two parallel ALE populations were initiated from independent clones of each of the three parental strains: K.p.Mut⁻fld::Adh_sm (K.p.ALE1), K.p.Mut⁻fld::Adh_cr (K.p.ALE2), and O.p.Mut⁻fld::Adh (O.p.ALE). Populations were maintained by serial batch cultivation for 81–87 days (10–12 passages) (Fig. 4 A). Over the course of the experiment, approximately 30 and 50 generations (biomass doublings) were achieved for *K. phaffii* and *O. parapolymorpha*, respectively.

Growth performance, assessed as both the overall specific growth rate over each passage ($\mu_{overall}$) and the maximum growth rate between sampling points within a passage (μ_{max}), improved progressively throughout the evolution (Fig. 4B). Parallel populations derived from the same parental strain exhibited highly similar growth trajectories, whereas populations originating from different strains displayed distinct adaptation profiles. K.p.ALE1 populations showed minimal improvement in $\mu_{overall}$ during the first five passages, followed by steady enhancement thereafter. In contrast, K.p.ALE2 populations exhibited rapid early gains in $\mu_{overall}$ that plateaued later in the experiment. However, μ_{max} values indicated continued incremental improvements in these populations until the end of the evolution period. Both O.p.ALE populations displayed higher initial growth rates and sustained improvement, resulting in a greater total number of generations within a shorter timeframe.

To characterize evolved phenotypes at the clonal level, three individual clones were isolated from each of the six evolved populations and assessed for growth on methanol in YNB shake-flask cultivations (Fig. 4 C). Although variability among clones was observed, all displayed improved growth relative to their respective parental strains. The maximum specific growth rates achieved after adaptive laboratory evolution represent a significant improvement over the initial engineered strains. The fastest-growing clone from each population (bold lines in Fig. 4 C) was selected for whole-genome sequencing. Among these, K.p.ALE1.2 clone 3 ($\mu_{max} = 0.038$ h^{-1}, $\mu_{overall} = 0.025$ h^{-1}) and O.p.ALE.1 clone 2 ($\mu_{max} = 0.044$ h^{-1}, $\mu_{overall} = 0.031$ h^{-1}) were chosen for further evaluation of carbon efficiency in chemostat cultivations.

2.4. Adh-based methanol growth increases biomass yield and reduces CO_2 emission

Methanol-limited chemostat experiments were conducted at a dilution rate of 0.02 h^{-1} to compare carbon efficiencies of evolved Mut⁻fld::Adh strains with their respective wild-type (WT) counterparts. Following an initial batch phase to reach $OD_{600} \approx 30$, continuous methanol feeding was initiated. Steady state was achieved after 5 days and maintained for an additional 10 days, corresponding to five reactor volume changes (Fig. 5 A,B). At steady state, the evolved *K. phaffii* strain K.p.ALE1.2 and the evolved *O. parapolymorpha* strain O.p.ALE.1 exhibited 52% and 49% reductions in specific CO_2 production rate (q_{CO2}), respectively, while maintaining biomass formation rates (q_X) comparable to their wild-type counterparts (Table 2). Because both evolved strains exhibited incomplete methanol consumption under steady-state conditions, a cell-free bioreactor experiment was performed to quantify methanol evaporation (Supplementary Fig. S3). Evaporation rates (mol MeOH h^{-1}) were determined at 30 °C and 37 °C using initial methanol concentrations of 0.5%, 1%, and 2% (vol vol^{-1}). A standard curve was generated to estimate evaporation as a function of concentration and temperature, revealing increased methanol loss at higher

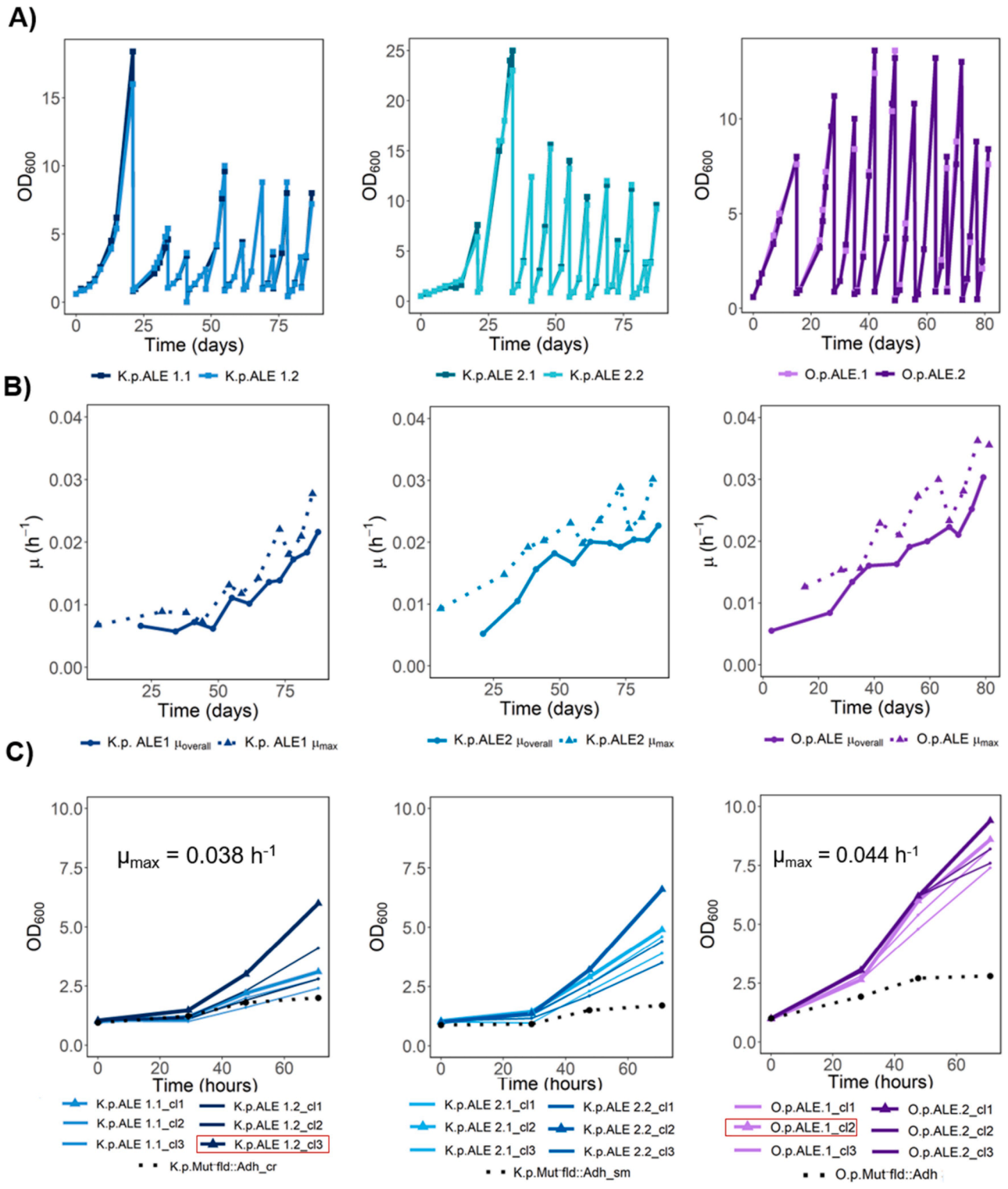

Fig. 4. Adaptive laboratory evolution of Mut⁻fld::Adh *K. phaffii* (K.p.) and *O. parapolymorpha* (O.p.) strains for improved growth on methanol. A) Optical density at 600 nm (OD_{600}) trajectories normalized to the initial OD_{600} of each population at the start of the ALE experiment during serial batch cultivation. Dark and light-colored lines represent independent parallel populations (XX.1 and XX.2) derived from the same parental strain. B) Overall ($\mu_{overall}$) and maximum (μ_{max}) specific growth rates for each passage. $\mu_{overall}$ values were calculated from the initial and final OD_{600} measurements of each passage and are plotted at the end of the corresponding passage. μ_{max} values were calculated from the pair of consecutive sampling points yielding the highest specific growth rate and are plotted at the time point at which they occurred. Data represent the mean of two parallel populations. C) Growth profiles of three isolated clones from each evolved population in YNB shake-flask cultivation on methanol. OD_{600} values were normalized to the initial OD_{600} of each culture. Data for the parental clone of each ALE population are shown as a black dotted line. Thick lines with triangle markers denote the clone from each population selected for genome sequencing. The red box highlights the clone selected for further characterization in chemostat experiments. The μ_{max} values shown correspond to the chemostat-selected clones and were calculated from the OD_{600} measurements between 29 and 48 h.

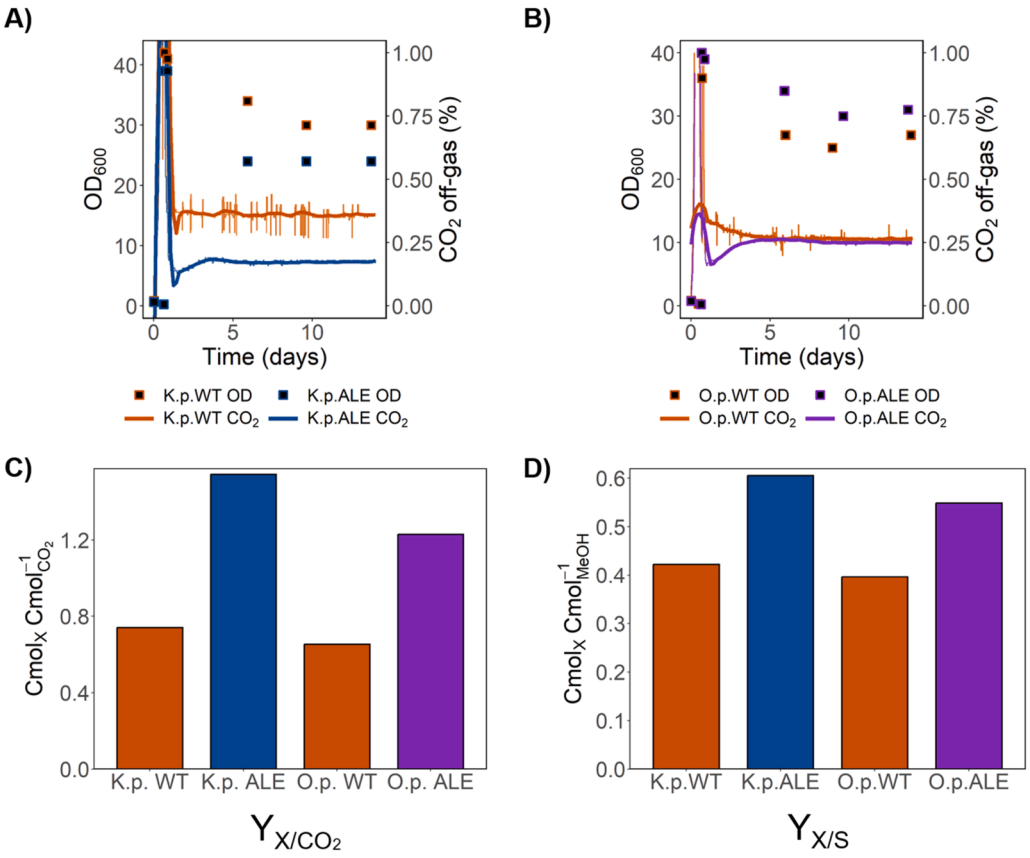

Fig. 5. Chemostat analysis of carbon efficiency in evolved Mut⁻fld::Adh (ALE) and wild-type (WT) strains of *K. phaffii* (K.p.) and *O. parapolymorpha* (O.p.). A) Offline OD measurements and online CO_2% offgas data for A) *K. phaffii* and B) *O. parapolymorpha.* C) Carbon efficiency expressed as biomass yield per CO_2 produced (Y_{X/CO_2}; Cmol Cmol^{-1}), D) Biomass yield on methanol (Y_{X/CO_2}; Cmol Cmol^{-1}). Yield values were calculated from steady-state data (day 14). Values for Mut⁻fld::Adh strains in panel D include correction for methanol evaporation rates determined in Supplementary Fig. S3. The strains labeled K.p.ALE and O.p.ALE are evolved Mut⁻fld::Adh strains K.p.ALE1.2 and O.p.ALE.1 from Table 1.

Table 2
Steady-state chemostat parameters for wild-type (WT) and evolved Mut⁻fld::Adh strains at a dilution rate of 0.02 h^{-1} .

Strain[a]	q_{CO2}	q_X	q_{MeOH}[b]	$Y_{X/S}$[b]
	mmol g^{-1} h^{-1}	Cmmol g^{-1} h^{-1}	mmol g^{-1} h^{-1}	g g^{-1}
K.p. WT	1.041	0.772	−1.813	0.344
K.p. ALE	0.503	0.777	−1.280	0.479
O.p. WT	1.225	0.801	−2.020	0.314
O.p. ALE	0.655	0.807	−1.462	0.434

[a] The strains labeled K.p.ALE and O.p.ALE are evolved Mut⁻fld::Adh strains K.p.ALE1.2 and O.p.ALE.1 from Table 1.

[b] Values for q_{MeOH} and $Y_{X/S}$ have been adjusted for methanol evaporation using the rate calculated in Supplementary Figure S3.

concentrations and temperatures (Supplementary Fig. S3A). Applying the calculated evaporation rates—0.0078 mol h^{-1} for 0.5% MeOH at 30 °C (*K. phaffii*) and 0.00385 mol h^{-1} for 0.15% MeOH at 37 °C (*O. parapolymorpha*)—resulted in carbon balances exceeding 99.5% closure for all strains (Supplementary Fig. S3B, C). These corrections were incorporated into reported q_{MeOH} and biomass yield ($Y_{X/S}$) values (Table 2, Fig. 5D). After correction, K.p.ALE1.2 displayed a 30% reduction in q_{MeOH} and a 43% increase in $Y_{X/S}$ relative to WT, in alignment with the predicted yields from FBA (Table S2), where a 32% reduction in q_{MeOH} and 47% increase in $Y_{X/S}$ was estimated.

Similarly, O.p.ALE.1 showed a 28% reduction in q_{MeOH} and a 38% increase in $Y_{X/S}$ compared with its WT counterpart. To assess carbon efficiency independently of methanol evaporation estimates, we also evaluated the biomass yield per CO_2 produced (Y_{X/CO_2}) (Fig. 5 C). For *K. phaffii*, Y_{X/CO_2} increased from 0.74 Cmol mol^{-1} in WT to 1.54 Cmol mol^{-1} in K.p.ALE1.2. A comparable improvement was observed in *O. parapolymorpha*, with Y_{X/CO_2} increasing from 0.65 to 1.23 Cmol mol^{-1} in O.p.ALE.1. Values greater than one indicate that more carbon is directed toward biomass formation than released as CO_2. Collectively, these results demonstrate that evolved Mut⁻fld::Adh strains channel a substantially larger fraction of methanol-derived carbon toward biomass production, whereas WT strains dissipate the majority as CO_2.

2.5. ALE leads to mutations affecting peroxisomal protein import

Genomic DNA was isolated from six evolved clones and their three corresponding parental strains (Fig. 4 C). Libraries were prepared and sequenced using Illumina NovaSeq X platform, and reads were mapped to the reference genomes of *K. phaffii* and *O. parapolymorpha* [51,54]. Coding mutations present in evolved clones but absent in the parental strains, and resulting in amino acid substitutions, truncations, or deletions, were further analyzed (Table 3). The most prominent mutations occurred in peroxin (PEX) genes, specifically *PEX5* and *PEX6*. Independent missense, nonsense, or deletion mutations in either *PEX5* or *PEX6* were identified in all four evolved *K. phaffii* strains and in one of the two evolved *O. parapolymorpha* strains. Pex5 and Pex6 are essential components of the peroxisomal protein import machinery in methylotrophic yeasts [55,56]. These mutations are therefore predicted to impair peroxisomal import, potentially redistributing XuMP cycle enzymes from the peroxisome to the cytosol (Fig. 6). Such relocalization would co-localize formaldehyde production by cytosolic Adh2 with the assimilatory pathway, providing a mechanistic explanation for the improved Adh-based methylotrophic growth observed in the evolved

Table 3
Coding sequence mutations found in evolved strains.

Strain	Gene name	Gene description	Protein change[a]	Mutation type
K.p. ALE1.1	*CBC2*	mRNA cap binding complex	S24Y	Missense
K.p. ALE1.1	*PEX6*	Peroxisomal membrane protein	G309fs	Frameshift deletion
K.p. ALE1.2	*PEX5*	Peroxisomal membrane protein	G331L	Missense
K.p. ALE1.2	rRNA	26S ribosomal RNA	————----	Genomic insertion
K.p. ALE2.1	*PEX6*	Peroxisomal membrane protein	E831fs	Frameshift insertion
K.p. ALE2.1	*PRR1*	pheromone-response regulator	V386fs	Frameshift insertion
K.p. ALE2.1	rRNA	26S ribosomal RNA	————----	Genomic insertion
K.p. ALE2.2	*PEX5*	Peroxisomal membrane protein	T515fs	Frameshift insertion
K.p. ALE2.2	rRNA	26S ribosomal RNA	————----	Genomic deletion
O.p. ALE.1	*NUP1*	Component of the nuclear pore complex	K8del	Frameshift deletion
O.p. ALE.2	*NUP1*	Component of the nuclear pore complex	K8del	Frameshift deletion
O.p. ALE.2	*SNF3*	High-affinity glucose transporter	F398L	Missense
O.p. ALE.2	*IRA1*	Inhibitory regulator protein I	N2470fs	Frameshift deletion
O.p. ALE.2	*PEX6*	Peroxisomal membrane protein	S561*	Nonsense

[a] Protein changes are reported using standard amino acid notation (OriginalAA Position NewAA). fs = frameshift; * = stop codon. All insertion and deletion mutations resulted in frameshifts and are predicted to produce non-functional proteins unless otherwise indicated. Further information on genomic position and alterations for mutations at the nucleotide level can be found in Supplementary Table S4.

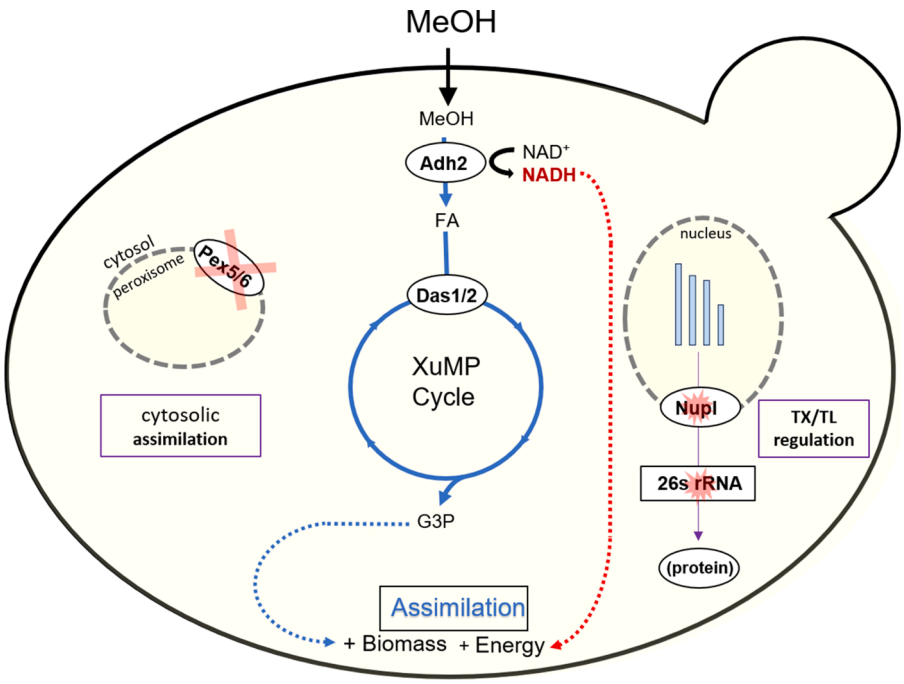

Fig. 6. Proposed functional consequences of recurrent mutations identified in evolved Mut⁻fld::Adh strains. Mutations in *PEX5* or *PEX6* are predicted to impair peroxisomal protein import, resulting in cytosolic relocalization of XuMP cycle enzymes in both *K. phaffii* (K.p.) and *O. parapolymorpha* (O.p.). This relocalization is proposed to co-localize formaldehyde production by Adh2 with the assimilatory pathway. Mutations in *NUP1* (O.p.) and 26S rDNA (K.p.) are proposed to affect gene regulation at the transcriptional (TX) and translational (TL) levels, respectively. Red crosses indicate predicted loss of protein function, and red stars denote proposed modulation of activity.

strains. To assess whether peroxisomal protein import was impaired, two evolved *K. phaffii* strains (K.p.ALE1.2 and K.p.ALE2.1) were transformed with an eGFP reporter fused to a C-terminal SKL peroxisomal targeting sequence (PTS1) (Supplementary Fig. S4). In the parental strains (K.p.Mut⁻fld::Adh_cr and K.p.Mut⁻fld::Adh_sm), eGFP–SKL exhibited punctate fluorescence consistent with peroxisomal localization. In contrast, the evolved strains displayed increased cytosolic fluorescence, indicating partial mislocalization of the reporter. Cytosolic localization was moderate in K.p.ALE1.2 and pronounced in K.p.ALE2.1, consistent with impaired peroxisomal import.

Additional recurrent mutations were identified in genes potentially affecting global regulation. In *K. phaffii*, a locus annotated as 26S rDNA (Chr3–1238) was mutated in three of the four evolved strains, with two strains carrying identical mutations. The read depth (DP, total number of sequencing reads that covered a specific genomic position) for these mutations was lower than for other variants (Supplementary Table S4). A lower DP generally indicates lower confidence or greater difficulty in mapping reads to that region. This is consistent with the highly repetitive nature of rDNA arrays, which complicates read mapping in short-read sequencing datasets [57].

The repeated targeting of this locus is notable given that *K. phaffii* contains approximately 16–29 copies of the 26S rDNA sequence [54,58]. The mutations may alter primarily translational capacity by affecting ribosomal RNA integrity. Alternatively, because they occur within the highly repetitive rDNA locus, they could influence rDNA transcription or chromatin organization, with broader consequences for global gene expression [59,60]. In *O. parapolymorpha*, both evolved strains independently acquired an identical deletion in *NUP1* (HPODL_01331). In *S. cerevisiae*, Nup1 is an essential component of the nuclear pore complex and has been implicated in transcriptional regulation [61]. However,

genome annotation of HPODL_01331 in *O. parapolymorpha* appears incomplete, lacking an annotated start codon, complicating functional interpretation. The consequences of the 26S rDNA and *NUP1* mutations remain unclear, but both are likely to influence gene expression, although the underlying regulatory mechanisms remain unknown. Further investigation will be required to determine their contribution to improved Adh-based methylotrophic growth.

2.6. Adh-based methanol assimilation increases itaconic acid yield

In parallel with adaptive laboratory evolution, we evaluated the potential of Mut⁻fld::Adh strains for organic acid production. Previously published *K. phaffii* strains capable of high-titer itaconic acid (ITA) production from methanol were used as a starting point [32]. To generate Mut⁻ derivatives, *AOX2* was first deleted using CRISPR–Cas9. Subsequently, the *AOX1* coding sequence was replaced with the native *ADH2* coding sequence and *FLD1* was deleted, yielding the strain ITA-Mut⁻fld::Adh. As an Aox-based comparison, *AOX1* was deleted in the parental ITA (Mut^{+}) strain, creating ITA-Mut^{S} strain with a single copy of Aox2. The metabolic configurations of the strains are summarized in Fig. 7A,B. Because both engineered strains exhibited lower growth rates than the Mut^{+} parental strains, cultivations were initiated at high cell density to better assess conversion efficiency. Following a batch phase and glycerol feed, biomass concentrations of ~45 g L^{-1} were achieved for both strains prior to methanol feeding. During the methanol phase, growth was minimal and comparable between strains (Fig. 7 C). However, ITA-Mut⁻fld::Adh produced 14.9 g L^{-1} itaconic acid, whereas ITA-Mut^{S} produced 10.3 g L^{-1} (Fig. 7D).

The product yield ($Y_{P/S}$) remained consistently higher for ITA-Mut⁻fld::Adh throughout the cultivation (Fig. 7D). The average $Y_{P/S}$ for ITA-Mut⁻fld::Adh was 0.119 g g^{-1} , compared with 0.065 g g^{-1} for ITA-Mut^{S}. To account for differences in biomass formation, total carbon conversion was evaluated by calculating the combined Cmoles directed toward biomass (X) and itaconate (ITA). Total converted X + ITA carbon was comparable between strains: 0.220 Cmol (0.086 Cmol X + 0.134 Cmol ITA) for ITA-Mut^{S} and 0.227Cmol (0.032 Cmol X + 0.194 Cmol ITA) for ITA-Mut⁻fld::Adh. However, total CO_2 production was lower in ITA-Mut⁻fld::Adh (0.679 Cmol) than in ITA-Mut^{S} (0.824 Cmol), resulting in an approximately 21% higher combined biomass and itaconate yield per mole of CO_2 produced ($Y_{(X+ITA)/CO_2}$, Cmol mol^{-1}) for the Adh-based strain.

Together, these results demonstrate that Adh-based methanol assimilation can support gram-per-liter-scale production of itaconic acid with improved product yield and reduced CO_2 evolution relative to the equivalent Mut^{S} strain. Importantly, the ITA-Mut⁻fld::Adh strain characterized here does not contain the *PEX5* or *PEX6* mutations identified

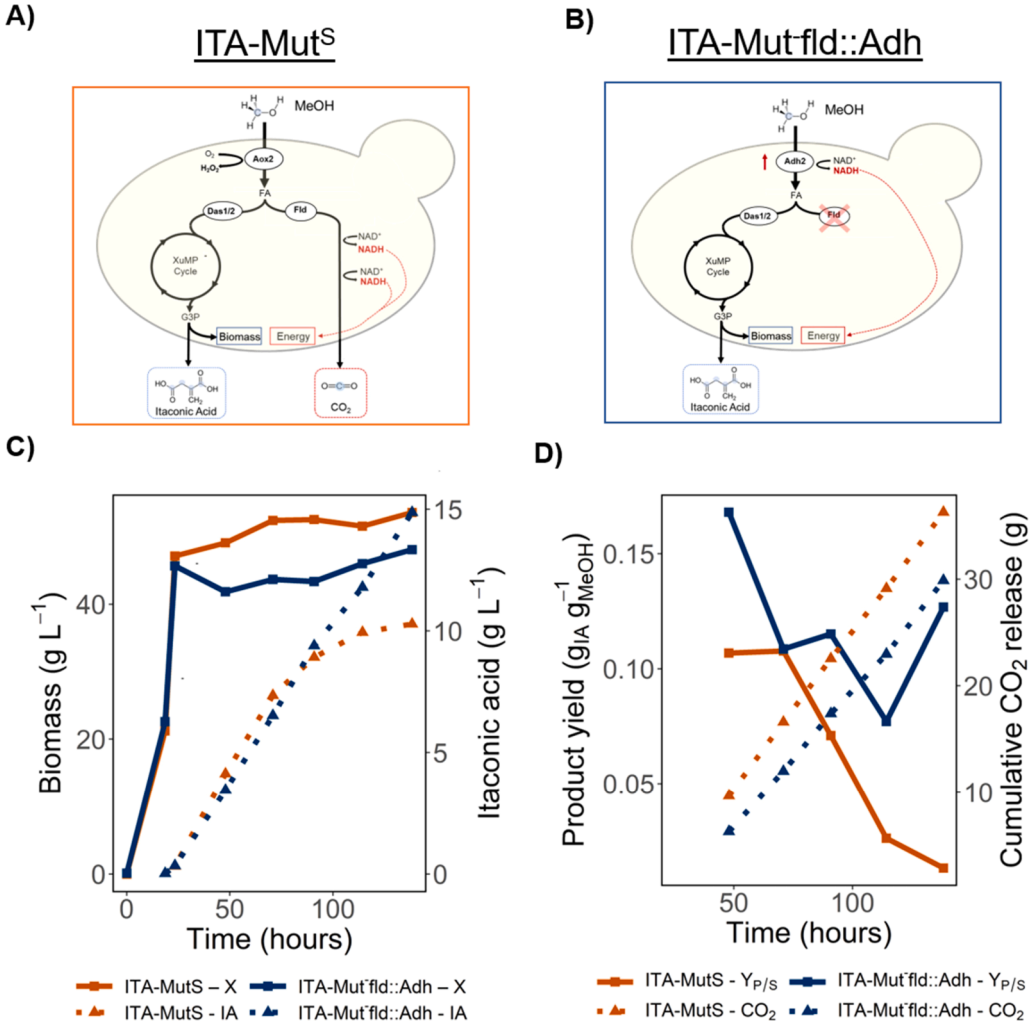

Fig. 7. Fed-batch bioreactor cultivations of engineered strains for itaconic acid production. A,B) Metabolic map for strains ITA-Mut^{S} and ITA-Mut⁻fld::Adh, constructed from strains previously engineered by Severinsen et al. [32]. C) Offline measurements of biomass and itaconic acid. D) Calculated product yield ($Y_{P/S}$) for conversion of methanol to itaconic acid, and cumulative CO_2 released over the course of cultivation. Calculation of $Y_{P/S}$ values did not incorporate a methanol evaporation estimate.

through ALE, suggesting that further gains in production efficiency may be achievable through combined engineering and evolutionary strategies.

2.7. Discussion

Some of the largest scale industrial biotechnology processes to date are performed with yeasts [62]. The ability of established industrial yeasts to grow on methanol offers a promising route toward a single-carbon bioeconomy. However, the inherent energy loss associated with alcohol oxidase (Aox)-mediated methanol oxidation constrains biomass and product yields.

Here, we demonstrate that deletion of formaldehyde dehydrogenase enables sustained Adh2-based growth in Mut$^-$ strains of both *K. phaffii* and *O. parapolymorpha*. To our knowledge, this represents the first example of a methylotrophic yeast capable of growth on methanol as the sole carbon and energy source in the absence of functional *AOX* genes [20]. Growth rates of Mut$^-$fld::Adh strains increased two- to threefold during approximately three months of adaptive laboratory evolution (ALE) (Fig. 3, Fig. 4). Recurrent mutations in *PEX5* and *PEX6* in both species identify peroxisomal import as key adaptation targets (Table 3). Chemostat experiments confirmed that evolved Mut$^-$fld::Adh strains exhibit reduced q_{CO_2} and increased biomass yield ($Y_{X/S}$) relative to wild type, demonstrating improved carbon efficiency (Fig. 5).

Our observation that deletion of *FLD1* abolishes methanol growth in wild-type *K. phaffii* is consistent with earlier work in *K. phaffii* and *Candida boidinii* [63,64], but differs from some recent reports in *K. phaffii*. Two studies examining *FLD1* disruption in the GS115 background reported residual growth on methanol. In one case, growth of the Δ*fld1* strain was strongly impaired relative to wild type, although the use of complex medium containing yeast extract (BMMY) complicates interpretation of methanol-dependent growth [65]. Another study reported near wild-type growth of a Δ*fld1* strain [66]. In contrast, we consistently observed no growth of Δ*fld1* strains on minimal methanol medium across two genetic backgrounds (CBS2612 and CBS7435) and two independent engineering strategies (split-marker recombination and CRISPR–Cas9), and tested across multiple methanol concentrations (Supplementary Fig. S2). These results support the prevailing view that the dissimilatory pathway is essential for energy generation in wild-type methylotrophic yeasts. Li et al. also explored both the Δ*fld* and Mut$^-$ phenotypes with *ADH900* overexpression in *K. phaffii* [67]. However these alterations were not combined, and therefore robust growth was not observed, and their work focused on the co-overexpression of Adh in the presence of Aox.

Although Mut$^-$ (Δ*aox1 aox2*) strains are unable to grow on methanol even when *ADH2* is overexpressed, the combination of Mut$^-$ and Δ*fld* enables growth in both *K. phaffii* and *O. parapolymorpha*. We propose that Adh2-mediated NAD-dependent methanol oxidation compensates for loss of the dissimilatory branch by maintaining cytosolic NADH generation comparable to that produced during formaldehyde dissimilation (Supplementary Fig. S1). The observation that the same phenotype—restoration of growth in Mut$^-$ strains upon *FLD1* disruption—occurs in two phylogenetically distinct methylotrophic yeasts suggests that Adh-based methylotrophy represents a generalizable metabolic configuration.

Recent efforts in synthetic methylotrophy have also produced methanol-utilizing *S. cerevisiae* strains involving native Adh2 and Δ*fld* phenotypes. Zhan et al. engineered XuMP-based growth in *S. cerevisiae* with a μ_{max} of 0.051 h^{-1} , although a cytosolic alcohol oxidase remained required for methanol oxidation [68]. Guo et al. used evolutionary engineering to obtain methanol-dependent growth in *S. cerevisiae* from strains initially expressing *K. phaffii* XuMP genes (*AOX1*, *DAS2*, *DAK2*, and *CTA1*), but these genes were subsequently lost during evolution, with growth proposed to proceed through a native Adh2–Sfa1–rGly pathway [69]. In contrast to our system, these strains retained active formaldehyde dehydrogenase and lacked a functional XuMP cycle, and no assessment of improved carbon efficiency was made.

Methanol-dependent growth via reductive glycine (rGly) pathway variants has also recently been demonstrated in *K. phaffii*, although both studies retained alcohol oxidase–mediated methanol oxidation [70,71]. Reported biomass yields for rGly-based strains (0.066 gDCW gMeOH^{-1} at $\mu = 0.019$ h^{-1}) are substantially lower than the 0.480 gDCW gMeOH^{-1} at $\mu = 0.020$ h^{-1} observed for evolved K.p.Mut$^-$fld::Adh strains here, although differences in cultivation mode and lack of evaporation correction complicate direct comparison. Theoretical carbon efficiencies of Adh-rGly and Mut$^-$fld::Adh (Adh–XuMP) configurations are comparable. Conversion of methanol to pyruvate via rGly permits net CO_2 fixation with ~0.5 ATP produced, whereas the Mut$^-$fld::Adh pathway eliminates CO_2 release and yields ~9 ATP surplus (Supplementary Table S3). Flux balance analyses performed in *E. coli* likewise identify Mdh–XuMP and Mdh–rGly as among the most efficient C1 assimilation strategies, with Mdh–XuMP predicted to be slightly superior [7]. Recently, *K. phaffii* strains growing via an Aox-RuMP configuration were described [72]. Among known methanol assimilation pathways, Adh–RuMP is predicted to achieve the highest theoretical biomass yield [7]. Combining these strategies could therefore enable highly energy-efficient production in *K. phaffii*, particularly when paired with an appropriately energy-demanding heterologous pathway. Together, these comparisons highlight Adh-based methylotrophy as a highly efficient strategy for improving C1 conversion efficiency in yeast and motivate further exploration of these pathways for industrial bioprocessing.

Isolated clones from the ALE experiment reached a maximum growth rate of 0.038 and 0.044 h^{-1} for *K. phaffii* and *O. parapolymorpha*. Although these rates remain lower than the typical growth rate observed for wild-type AOX-based growth (~0.12–0.15 h^{-1}), they are comparable to the industrially relevant Mut^S phenotype (0.04 h^{-1}) commonly used for protein production [73–75]. The continued increase in growth rates throughout the ALE experiment suggests that further improvement of Mut$^-$fld::Adh strains remains possible (Fig. 4B). Extending the evolution experiment with either the evolving populations or selected high-performing clones therefore represents a promising direction. Reverse engineering of the identified PEX mutations in parental strains would also help confirm their beneficial role in Adh2-based growth while providing improved starting points for further evolution. Faster-growing strains may additionally enable chemostat experiments in which methanol is fully consumed, avoiding the need to estimate methanol evaporation rates.

The inability of evolved Mut$^-$fld::Adh strains to completely consume methanol during chemostat cultivation may also reflect the relatively low affinity of native Adh2 for methanol. The K_m values determined here for *K. phaffii* Adh2 (135–190 mM) lie at the upper end of the reported range for bacterial methanol dehydrogenases (21–150 mM), yet remain substantially higher than those of yeast alcohol oxidases (0.4–4 mM) [76–78]. Although heterologous expression of bacterial methanol dehydrogenases could in principle improve methanol oxidation, previous efforts in *K. phaffii* and *S. cerevisiae* have shown poor in vivo performance, likely due to challenges in expression or enzyme activity in the yeast cellular context [68,79]. Engineering yeast alcohol dehydrogenases with improved methanol activity therefore represents a promising direction to further enhance Adh-based methylotrophy.

The biomass yield of 0.48 g g^{-1} observed for evolved Mut$^-$fld::Adh *K. phaffii* strains is, to our knowledge, the highest reported for a yeast growing on methanol and approaches the yields of Gram-positive methylotrophic bacteria (0.50–0.55 g g^{-1}). The yield calculated here for wild-type *K. phaffii* (0.33 g g^{-1}) is slightly lower than previously reported values (~0.38 g g^{-1} at $\mu = 0.035$ h^{-1}), consistent with the observation that biomass yield decreases at lower growth rates in methanol-limited chemostats (Table 2) [40]. The experimentally determined physiological parameters also agreed well with the FBA predictions, with similar relative improvements in biomass yield (+48% predicted vs. +43% experimental), methanol uptake (−32% vs. −29%),

and CO_2 production (−48% vs. −52%) (Table 2, Supplementary Table S1). The differences in absolute values may partly reflect the estimated non-growth-associated maintenance energy (NGAME), which has experimental variation among studies with *K. phaffii* and has a proportionally greater influence on flux predictions at low growth rates [40,72].

Similarly, the yield of 0.43 g g^{-1} observed for evolved Mut$^-$fld::Adh *O. parapolymorpha* strains represents the highest reported for this species (Table 2). Although slightly lower than in *K. phaffii*, this result is consistent with earlier studies showing relatively lower biomass yield for *O. parapolymorpha* [80]. However, the higher thermotolerance of *O. parapolymorpha* and high growth rates makes it an interesting host to further develop for Adh-based growth and bioproduction. The biomass yields reported here were corrected for methanol evaporation to establish carbon balances and compare the intrinsic biological carbon conversion efficiency of the engineered strains. We acknowledge, however, that methanol evaporation in large-scale fermentations will need to be minimized through appropriate engineering solutions, such as off-gas methanol recovery and recycling, to avoid substrate losses that compromise the overall process yield. To complement the widely reported $Y_{X/S}$ metric, we also quantified biomass produced per CO_2 emitted (Y_{X/CO_2}), which provides an additional measure of carbon efficiency that is independent of methanol evaporation and likewise demonstrates the improved carbon efficiency of the evolved strains (Fig. 5). The Mut$^-$fld::Adh strains produced approximately half as much CO_2 as the parental strains (Table 2), a change that could substantially improve the life-cycle assessment of methanol-based bioprocesses. In processes where CO_2 is vented, reduced emissions directly lower the carbon footprint. In systems where CO_2 is captured and recycled to methanol, lower CO_2 generation would reduce both the energy demand and capital costs associated with carbon recycling.

Beyond improvements in carbon efficiency, replacing an oxidase with an NADH-dependent dehydrogenase offers industrial advantages regarding process economics. Native Aox-mediated methanol oxidation is highly exothermic and consumes one mole of oxygen directly per mole of methanol processed. Although half a mole of oxygen is effectively recovered through the catalase reaction, the native pathway still imposes a substantially higher oxygen demand than the Adh-based pathway, which conserves the reducing power as NADH and avoids direct oxygen consumption during the initial oxidation step. This was confirmed by the FBA, which predicted an approximately 50% reduction in the specific oxygen uptake rate for the Mut$^-$fld::Adh strains compared to the wild type (Supplementary Table S1). Industrially, this reduced oxygen demand translates to lower aeration and agitation requirements, which are major drivers of electricity costs [81]. The model also predicts a proportional reduction in metabolic heat generation (Supplementary Table S1), suggesting lower cooling requirements and associated energy costs during large-scale cultivation.

Notably, mutations in *PEX5* were also reported in previous work evolving autotrophic, Aox-based *K. phaffii* strains, where they were shown to enhance peroxisomal import [82]. In that context, increased import is consistent with the peroxisomal localization of both Aox and CBB pathway enzymes. In contrast, we demonstrate that mutations arising in PEX genes of evolved Mut$^-$fld::Adh strains impair peroxisomal import of SKL-tagged proteins, presumably promoting cytosolic localization (Table 3, Supplementary Fig. S4). This redistribution may confer a selective advantage under Adh-based methylotrophy by co-localizing cytosolic methanol oxidation with the assimilatory pathway. In this context it should be noted that we have previously attempted to co-localize Adh2 with assimilation in the peroxisome, however unsuccessfully, leading to the conclusion that Adh2 needs the cytosolic context for activity [46]. Concurrent interruption of the dissimilatory branch avoids competition with assimilation and allows growth, a metabolic state that may have been further strengthened during ALE by a redistribution of the assimilation pathway to the cytosol (Supplementary Fig. S1, Fig. 6). Interestingly, the *PEX6* mutation found in evolved clone ALE1.2 resulted in stronger cytosolic mislocalization of the SKL-tagged reporter compared to *PEX5* mutation found in evolved clone ALE2.1, and was associated with slower growth (Fig. 4 C, Supplementary Fig. S4). Pex5 is directly involved in protein import to peroxisomes while Pex6 mediates its retrograde export to the cytosol [83]. One possible explanation is that the *PEX5* missense mutation partially reduces protein import, whereas the *PEX6* frameshift mutation causes a stronger impairment of the import cycle, resulting in more pronounced cytosolic mislocalization. These observations suggest that partial retention of peroxisomal targeting for a subset of enzymes may be beneficial. Across the 4 evolved *K. phaffii* strains sequenced, the two *PEX5* mutants (K.p.ALE1.1 and K.p.ALE2.1) grew faster than the two *PEX6* mutants (K.p.ALE1.2 and K.p.ALE2.2) (Table 3, Fig. 4 C). However, because one of the additional *PEX5* alleles is also a frameshift mutation and only two strains were examined by fluorescence microscopy, it remains unclear whether this effect reflects the specific mutations or distinct roles of Pex5 and Pex6 in peroxisomal protein import.

The ITA-Mut$^-$fld::Adh strains described here demonstrate that the native Adh2 in *K. phaffii* can support gram-per-liter–scale production of organic acids from methanol. The itaconic acid titer was approximately twofold lower than in the parental Mut$^+$ strain under similar conditions and duration [32]. However the Mut$^-$fld::Adh system offers clear opportunities for improvement through both strain and process engineering. Incorporation of the identified PEX mutations, optimization of gene copy numbers, and further process optimization may substantially improve itaconic acid productivity. Notably, the product yield of ITA-Mut$^-$fld::Adh (0.12 g g^{-1}) exceeded that of the Mut^S strain (0.07 g g^{-1}) and was comparable to previously reported parental strain yields (0.09–0.14 g g^{-1}), despite higher methanol concentrations and longer cultivation times [32]. Accounting for methanol evaporation—which was not measured in these experiments—would likely further increase the biological yield advantage of Mut$^-$fld::Adh strains.

For commodity products such as food ingredients, organic acids, and bulk chemicals, improvements in carbon efficiency have a substantial impact on both the carbon footprint and economic viability of bioprocesses. Unlike typical metabolic engineering strategies that optimize flux partitioning between biomass and product formation, the approach demonstrated here targets the upstream branch point between carbon assimilation and CO_2 release. By eliminating the methanol dissimilation pathway and coupling NADH formation directly to assimilation, Adh-based methylotrophy minimizes carbon loss associated with energy generation. This strategy resembles the energetic coupling underlying ethanol fermentation in yeast and can be viewed as a form of growth-coupled production [48,84]. Mut$^-$fld::Adh strains may also prove advantageous for methanol-induced protein production processes, potentially enabling higher productivity than non-growing Mut$^-$ production strains, with comparable growth rates to industrial Mut^S phenotypes, while retaining the efficiency benefits of Adh-based methanol metabolism [43]. More broadly, this approach offers a general strategy to improve conversion efficiency in methylotrophic yeasts beyond product-specific or pathway optimization.

2.8. Concluding remarks

The present work demonstrates that carbon efficiency in industrial methylotrophic yeasts can be substantially improved through a combination of targeted metabolic engineering and adaptive laboratory evolution. The combination of two growth defective mutations creates a viable phenotype, forcing flux for energy production through the assimilatory pathway. The Adh-based metabolic configuration and the mutations identified here provide a foundation for developing a new generation of highly efficient yeast cell factories for the emerging single-carbon bioeconomy.

3. Methods

3.1. Metabolic modelling

Genome-scale metabolic modelling was performed in COBRApy using the iMT1026v3 model of *K. phaffii* [40]. Growth on methanol was simulated by constraining alternative carbon sources and enabling methanol uptake. To represent the engineered strain (Mut⁻fld::Adh), an NAD-dependent, cytosolic methanol oxidation reaction (Adh2) was introduced, while alcohol oxidase and formaldehyde dissimilation reactions were disabled. Flux balance analysis was performed using the GLPK exact solver by maximizing biomass formation or, at fixed specific growth rates (μ), by parsimonious flux balance analysis to determine associated flux distributions. Biomass yield ($Y_{X/S}$) was derived from μ and methanol uptake. The NGAME value for methanol growth (2.88 mmol ATP $gDCW^{-1}$ h^{-1}) was recalculated from the chemostat data reported by Kuzman et al., as this dataset represents methanol-limited growth over the low specific growth rate range considered here [72]. This value replaced the original NGAME of 0.44 mmol ATP $gDCW^{-1}$ h^{-1} reported by Tomàs-Gamisans et al., which was estimated from higher growth-rate data, while all other methanol-specific model constraints and parameters were retained [40]. The complete Python script used to generate the engineered model, define all model modifications and constraints, and perform the FBA is provided as a Supplementary File.

3.2. Strain construction

The parental strains of the present work are *Komagataella phaffii* (syn. *Pichia pastoris*) CBS2612 and *Ogataea parapolymorpha* DL1. *K. phaffii* CBS2612 Mut⁻ and Mut⁻ *ADH2* overexpression strains used as starting points in this study were previously generated by Zavec et al. [44]. All plasmid constructs were assembled using Golden Gate Assembly (GGA) as described previously [38].

Deletion of *FLD1* was performed using either a split-marker (SM) recombination cassette or CRISPR–Cas9-mediated genome editing. For SM-mediated deletion, the disruption cassette contained a geneticin resistance marker, and transformants were selected on YPD plates supplemented with 500 μg mL^{-1} geneticin. For CRISPR–Cas9 editing, a homologous donor DNA repair template with 500–1000 bp homology arms flanking the target site was supplied, as previously described [39]. The CRISPR plasmid contained a nourseothricin (NTC) resistance marker, and transformants were selected on YPD plates containing 100 μg mL^{-1} NTC. Following transformation, sequential streaking on non-selective YPD plates was performed to cure the CRISPR plasmid. Loss of the selection marker was confirmed for all *K. phaffii* strains. In contrast, both NTC and geneticin resistance persisted in *O. parapolymorpha* strains after multiple rounds of streaking on non-selective YPD plates. Gene deletions and coding sequence replacements were verified by polymerase chain reaction (PCR) amplification across the *FLD1* locus in *K. phaffii* and the *AOX/FLD* loci in *O. parapolymorpha*. A list of strains used in this study is provided in Table 1.

For itaconic acid production, the previously described *K. phaffii* CBS7435 ITA strain engineered by Severinsen et al. was used as the parental strain [32]. This strain carries genomically integrated expression cassettes for the *Aspergillus terreus* cis-aconitate decarboxylase (cadA), mitochondrial cis-aconitate transporter (mttA), and major facilitator superfamily itaconic acid exporter (mfsA), expressed under the *AOX1*, *POR1*, and GAP promoters, respectively. The derivative strains ITA-Mut^S and ITA-Mut⁻fld::Adh were subsequently constructed from this parental strain by sequential CRISPR–Cas9-mediated genome editing. The resulting genotypes are summarized in Table 1 and described in the Results section.

3.3. Shake flask cultivations

Unless otherwise stated, shake-flask cultivations were performed at 180 rpm. *K. phaffii* cultivations were carried out at 30 °C, whereas *O. parapolymorpha* cultivations were performed at 30, 37, or 40 °C, as indicated for the individual experiments. ALE cultivations were conducted in 250 mL shake flasks with a 20–25 mL working volume and ceramic breathable stoppers. YNB screening cultivations were performed in 100 mL shake flasks with a 15–20 mL working volume, while larger cotton-plugged shake flasks were used for precultures intended for bioreactor inoculation. For precultures, isolated colonies for each strain were inoculated in YPG (yeast extract 10 g L^{-1}, soy peptone 20 g L^{-1}, glycerol 20 g L^{-1}) with antibiotics (where appropriate) and grown overnight (~18 h). The preculture was washed twice with YNB (Difco BD, Approximate Formula: Vitamins: biotin 2 μg L^{-1}, calcium pantothenate 400 μg L^{-1}, folic acid 2 μg L^{-1}, inositol 2000 μg L^{-1}, niacin 400 μg L^{-1}, p-aminobenzoic acid 200 μg L^{-1}, pyridoxine hydrochloride 400 μg L^{-1}, riboflavin 200 μg L^{-1}, thiamine hydrochloride 400 μg L^{-1}. Compounds supplying trace elements: boric acid 500 μg L^{-1}, copper sulfate 40 μg L^{-1}, potassium iodide 100 μg L^{-1}, ferric chloride 200 μg L^{-1}, manganese sulfate 400 μg L^{-1}, sodium molybdate 200 μg L^{-1}, zinc sulfate 400 μg L^{-1}. Salts: monopotassium phosphate 1.0 g L^{-1}, magnesium sulfate 0.5 g L^{-1}, sodium chloride 0.1 g L^{-1}, calcium chloride 0.1 g L^{-1}) medium supplemented with 10 g L^{-1} $(NH_4)_2SO_4$ and 0.5% methanol, and the required volume for a starting optical density of 0.5 was transferred to a new flask with YNB medium supplemented with 10 g L^{-1} $(NH_4)_2SO_4$ and 2% methanol (vol vol^{-1}). Prior to sampling, mass of the flasks was measured to adjust for evaporation through sterile water addition. Sampling was performed every 1–3 days for measurement of optical density and methanol concentration. Methanol was measured with HPLC and used to estimate methanol feeding volume required to maintain close to 2% methanol (vol vol^{-1}).

3.4. Purification and in vitro characterization of alcohol dehydrogenase 2 (Adh2)

A *K. phaffii* CBS7435 strain expressing native alcohol dehydrogenase 2 (*ADH2*) with an N-terminal His tag was cultivated in YPD medium (yeast extract 10 g L^{-1}, soy peptone 20 g L^{-1}, glucose 20 g L^{-1}) under the constitutive pGAP promoter. Briefly, a 10 mL YPD preculture was grown for 9 h (25 °C, 180 rpm) and used to inoculate 100 mL YPD in a 1 L flask. After 15 h and 22 h of cultivation, glucose was added to final concentrations of 0.5% and 1% (w v^{-1}), respectively. Cells were harvested after an additional 24 h (4000 g, 10 min, 4 °C) and stored at −20 °C prior to lysis. For protein extraction, cell pellets were resuspended in PBS to a target OD_{600} of 60 and distributed into twelve 1.5 mL screw-cap tubes. Cells were pelleted (4000 g, 10 min, 4 °C), resuspended in extraction buffer, and mixed with an equal volume of sterile glass beads. Cells were disrupted using an MP FastPrep−24 instrument (three cycles, 20 s, 6.0 m s^{-1}) with cooling on ice between cycles. Lysates were clarified by centrifugation (13,000 g, 1 min), and the soluble fraction was collected for purification.

His-tagged Adh2 was purified by immobilized Ni^{2+} affinity chromatography using an ÄKTA purifier UPC 100 system (GE Healthcare) equipped with a 1 mL HisTrap HP column. Samples and buffers were filtered (0.45 μm), degassed, and adjusted to pH 7.4 prior to purification. Binding buffer consisted of PBS containing 40 mM imidazole and 0.5 M NaCl (pH 7.4), while the elution buffer contained PBS, 500 mM imidazole, and 0.5 M NaCl (pH 7.4). The clarified lysate was adjusted to match binding buffer composition prior to loading. Eluted fractions were analyzed by SDS–PAGE and subjected to buffer exchange using Amicon Ultra−15 centrifugal filter units (10 kDa cutoff) to remove imidazole. The buffer was exchanged to 20 mM HEPES containing 1.5 mM $MgCl_2$ (pH 7.4) through four sequential concentration steps, yielding a final protein volume of 1–2 mL. Protein concentration was

determined using a Pierce BCA assay. Glycerol (10%) was added as a cryoprotectant prior to storage at −20 °C. Protein purity and concentration were further assessed using a Caliper LabChip GXII Touch system (PerkinElmer) and NanoDrop spectrophotometry.

Enzyme activity assays were performed in 96-well plates using a microplate reader (Tecan). Reactions (300 µL total volume) contained 2 µg purified enzyme, supplemented with 2 mM NAD^+. Reaction buffers were 100 mM HEPES with 5 mM $MgCl_2$ (pH 7.5) or 100 mM MOPS with 5 mM $MgSO_4$ (pH 9.8). Samples were equilibrated for 10–15 min prior to initiation of the reaction by addition of methanol. Enzyme activity was determined by monitoring NADH formation at 340 nm using the extinction coefficient $\varepsilon_{340} = 6220\ M^{-1}\ cm^{-1}$. Temperature dependence of enzyme activity was measured between 30.0 and 42.5 °C in 2.5 °C intervals using 1 M methanol as substrate. Activity was expressed in mU mg^{-1} , where one unit corresponds to the conversion of 1 µmol substrate per minute. Kinetic parameters were determined by measuring initial rates across methanol concentrations ranging from 10 to 1000 mM over a 5 min interval. K_m and V_{max} values were obtained using Hanes–Woolf plots of substrate concentration versus substrate concentration divided by reaction rate. K_m and V_{max} were then calculated with the below equation, where [A] = methanol concentration (mM), v = initial reaction rate (µmol NADH min^{-1}), K_m = Michaelis constant (mM), V_{max} = Maximum reaction rate (µmol NADH min^{-1}).

$$\frac{[A]}{v} = \frac{K_M}{V_{max}} + \frac{[A]}{V_{max}}$$

3.5. HPLC measurements

Samples were vortexed and centrifuged at 16,100*g* for 5 min at room temperature. The supernatant was acidified with H_2SO_4 (40 mmol L^{-1} stock solution) to a final concentration of 4 mmol L^{-1} . Samples were centrifuged again and filtered through 0.22 µm syringe filters prior to HPLC analysis. Metabolite concentrations were determined using a Bio-Rad Aminex HPX-87H column (300 × 7.8 mm). The mobile phase consisted of 4 mmol L^{-1} H_2SO_4 with a flow rate of 0.6 mL min^{-1} at 60 °C. Methanol was detected using a refractive index detector (RID−10A, Shimadzu), while itaconic acid was quantified using a photodiode array detector (SPD-M20A, Shimadzu) at 254 nm.

3.6. Chemostat cultivations

Bioreactor cultivations were performed in 1.0 L DASGIP stirred-tank reactors (Eppendorf) with a working volume of 500 mL. Reactors were inoculated with 15 mL preculture into glycerol batch medium and cultivated until an OD_{600} of ~40 was reached. At the end of the batch phase, continuous cultivation was initiated with methanol chemostat medium at a dilution rate of 0.02 h^{-1} .

During chemostat operation, temperature was maintained at 30 °C for *K. phaffii* and 37 °C for *O. parapolymorpha*. Stirrer speed was set to 700 rpm, and pH was controlled at 6.0 using 12.5% NH_3. Air flow was set to 20 sL h^{-1} for most cultivations and 30 sL h^{-1} for *O. parapolymorpha* WT and cell-free control experiments. Dissolved oxygen was not actively controlled and ranged between 79–89% during steady-state cultivation. After five reactor volume changes, samples were collected at 330 h and 375 h after inoculation for steady-state analysis.

Methanol evaporation during chemostat cultivation was estimated using cell-free batch experiments. Four bioreactors (two at 30 °C and two at 37 °C) were filled with 500 mL methanol chemostat medium, and methanol was added to final concentrations of 0.5%, 1%, and 2% (v v^{-1}). Methanol concentrations were measured immediately after adjustment and again after 1 h under constant operating conditions. The measured losses were used to generate a standard curve describing methanol evaporation as a function of temperature and concentration (Supplementary Fig. S3).

Glycerol batch medium (per L): 46.5 g glycerol (86%), 4.4 g citric acid monohydrate, 13.5 g H_3PO_4 (85%), 0.5 g $CaCl_2{\cdot}2H_2O$, 9 g K_2SO_4, 2 g KOH, 0.5 g $MgSO_4{\cdot}7H_2O$, 8.7 mL biotin solution (0.1 g L^{-1}), and 4.6 mL trace element solution. The pH was adjusted to 6.0 using 32% (w w^{-1}) HCl.

Methanol chemostat medium (per L): 16.0 g methanol (2% v/v), 0.8 g citric acid, 6.6 g $(NH_4)_2HPO_4$, 0.01 g $CaCl_2{\cdot}2H_2O$, 0.76 g KCl, 0.3 g $MgSO_4{\cdot}7H_2O$, 1.22 mL biotin solution (0.1 g L^{-1}), and 0.74 mL trace element solution. The pH was adjusted to 6.0 with 32% (w w^{-1}) HCl.

Trace element solution (per L): 6.0 g $CuSO_4{\cdot}5H_2O$, 0.08 g NaI, 3.36 g $MnSO_4{\cdot}H_2O$, 0.2 g $Na_2MoO_4{\cdot}2H_2O$, 0.02 g H_3BO_3, 0.82 g $CoCl_2$, 20.0 g $ZnCl_2$, 65.0 g $FeSO_4{\cdot}7H_2O$, and 5.0 mL H_2SO_4 (95–98%).

3.7. Fed-batch cultivations

Fed-batch cultivations were performed in 1.0 L DASGIP stirred-tank reactors (Eppendorf) as previously described [32]. Reactors were inoculated with precultures grown overnight at 25 °C in glycerol batch medium. Precultures were initiated from 1 mL working cell bank stocks and cultivated in 100 mL medium, with 50 mL YPG added shortly before inoculation. Cells were used to inoculate the bioreactor batch phase at an initial OD_{600} of 1.

To reproduce the high-performing fermentation conditions described by Severinsen et al., a modified fed-batch strategy was applied to control biomass formation [32]. Dissolved oxygen was maintained at 30% by automated adjustment of stirrer speed, inlet gas flow, and oxygen concentration. Minimum setpoints were 200 rpm, 9.5 sL h^{-1} airflow, and 21% O_2, while maximum setpoints were 1250 rpm, 50 sL h^{-1} airflow, and 100% O_2. The pH was maintained at 5.5 using 5 M KOH to counteract acidification during cultivation.

The initial glycerol batch phase (~20 h) was followed by a 4 h limited glycerol feed phase (500 mL L^{-1} glycerol) without additional trace elements or biotin. This step was used to increase biomass to approximately 45 g L^{-1} and induce methanol-inducible gene expression. Subsequently, a limited methanol feed was initiated and supplemented with periodic methanol additions to maintain a concentration of approximately 2% (v v^{-1}). Samples were taken daily to measure methanol and itaconic acid concentrations.

Glycerol batch medium (modified BSM, per L): 18.5 g glycerol (86%), 2.0 g citric acid, 12.6 g $(NH_4)_2HPO_4$, 0.022 g $CaCl_2{\cdot}2H_2O$, 0.9 g KCl, 0.5 g $MgSO_4{\cdot}7H_2O$, 4 mL biotin solution (0.1 g L^{-1}), Glanapon 2000, 19.14 mL 25% NH_3, and 4.35 mL trace element solution (as described for chemostat medium).

3.8. Adaptive laboratory evolution

Adaptive laboratory evolution (ALE) was performed using serial batch cultivation as previously described [52,82]. Cultures were grown in 250 mL shake flasks with a working volume of 20–25 mL YNB medium supplemented with 10 g L^{-1} $(NH_4)_2SO_4$ and 2% (v v^{-1}) methanol. Each batch cycle was initiated at an OD_{600} of 0.5–1.0. Cultures were sampled every 2–3 days to monitor growth and methanol consumption. Once sufficient growth was observed, a new cultivation cycle was initiated by transferring an appropriate volume of culture to fresh medium to achieve a starting OD_{600} of 0.5–1.0. Methanol concentrations were maintained close to 2% (v v^{-1}) by periodic additions based on HPLC measurements.

3.9. Whole-genome sequencing

Genomic DNA from parental strains and evolved isolates was extracted as previously described [85]. DNA quality and concentration were assessed by agarose gel electrophoresis and UV absorbance at 260 and 280 nm.

Library preparation and sequencing were performed at the Vienna Biocenter Core Facility for Next Generation Sequencing using an Illumina NovaSeq X platform (10B XP flow cell, 2 × 150 bp paired-end

reads). Sequencing reads were mapped to *K. phaffii* strain CBS7435 (NCBI accession PRJEA62483) [86] or *O. parapolymorpha* DL1 (NCBI accession AEOI00000000) [51]. Variant calling was performed using Freebayes with parameters "–ploidy 1 –min-alternate-qsum 100 –min-alternate-fraction 0.8", corresponding to a minimum variant frequency of 80%. Variants were identified within annotated genes and 500 bp upstream and downstream regions. Sequencing data are available in the NCBI SRA under accession number PRJNA1405092, and complete variant calling output is provided as a supplementary file. Mutation analysis and annotation were performed using CLC Genomics Workbench v12.0 (QIAGEN).

3.10. Fluorescence microscopy

All strains were transformed with a plasmid expressing eGFP fused to a C-terminal PTS1 peroxisomal targeting sequence under control of the constitutive pGAP promoter. Strains were cultivated as described in Section 4.2 using YNB medium containing 1% (v v^{-1}) methanol. For microscopy, 5 µL of culture was transferred onto a glass microscope slide. Fluorescence imaging was performed using a Zeiss Axio Observer Z1/7 microscope equipped with an LCI Plan-Neofluar 63 × /1.3 objective and a 1.6 × tube lens. Differential interference contrast (DIC) images were acquired using a TL halogen lamp (6.1 V) with an exposure time of 190 ms. eGFP fluorescence was detected using excitation and emission filters of 450–490 nm and 500–550 nm, respectively. Illumination was provided by an LQ-HXP 120 lamp set to 80% intensity with an exposure time of 2.2 s. Images were acquired separately for DIC and fluorescence channels, and merged overlays were generated using Zeiss ZEN software.

Author contributions

D.M. and Ö.A. conceived and initiated the project. D.M., Ö.A. J.D. and C.M. designed the experiments. C.M., D.A. and L.H. constructed the strains. C.M., V.E., V.K., M.M.S., L.L. and M.B. carried out the experiments. B.C. and C.M. adapted the metabolic model and performed FBA calculations. C.M., Ö.A. and D.M. analysed the data. C.M., Ö.A. and D.M. wrote the manuscript. All authors read and approved the final manuscript.

CRediT authorship contribution statement

Charles Moritz: Data curation, Formal analysis, Investigation, Methodology, Visualization, Writing – original draft, Writing – review & editing. **Verena Enzinger:** Investigation. **Viktoria Kowarz:** Investigation. **Manja Mølgaard Severinsen:** Investigation, Methodology. **Lisa Lutz:** Investigation, Methodology. **Michael Baumschabl:** Investigation. **Daniel Ahlheit:** Investigation. **Benjamin L. Coltman:** Formal analysis, Methodology. **Luca Hodes:** Data curation, Methodology. **Jean-Marc Daran:** Supervision. **Özge Ata:** Conceptualization, Project administration, Supervision, Writing – original draft, Writing – review & editing. **Diethard Mattanovich:** Conceptualization, Funding acquisition, Supervision, Writing – original draft, Writing – review & editing.

Declaration of Competing Interest

D.M. is a co-founder of NewPathBio GmbH which develops methanol-based bioprocesses with yeasts. The other authors declare no conflict of interest.

Acknowledgements

The COMET center acib: Next Generation Bioproduction is funded by BMIMI, BMWET, SFG, Standortagentur Tirol, Government of Lower Austria and Vienna Business Agency in the framework of COMET – Competence Centers for Excellent Technologies. The COMET Funding Program is managed by the Austrian Research Promotion Agency FFG. We thank the Austrian Science Fund for support to D.M., C.M. and D.A. (Grant-DOI 10.55776/W1224, Doctoral Program on Biomolecular Technology of Proteins (BioToP)), and to D.M. and Ö.A. (FWF Excellence Cluster COE 17, Circular Bioengineering (Funding DOI: 10.55776/CO17)). M.M.S. was supported by the project 'Innovative bio-based chains for CO_2 valorisation as added-value organic acids'—VIVALDI (ID: 101000441) from the Horizon 2020 Program of the European Commission; 2017-SGR-1462 and by the Bioprocess Engineering Doctoral School of BOKU University. We are grateful to Petr Vojta for performing the Illumina WGS analysis. The equipment for this work was kindly provided by the BOKU Core Facility "Bioinformatics" (BINF).

Appendix A. Supporting information

Supplementary data associated with this article can be found in the online version at doi:10.1016/j.nbt.2026.08.006.

Data availability

Data will be made available on request.

References

[1] Vorholt JA. Microbial life in the phyllosphere. Nat Rev Microbiol 2012;10:828–40.
[2] Wegner G. Emerging applications of the methylotrophie yeasts. FEMS Microbiol Rev 1990;87:279–83.
[3] Cereghino JL, Cregg JM. Heterologous protein expression in the methylotrophic yeast Pichia pastoris. FEMS Microbiol Rev 2000;24:45–66.
[4] Solomons GL. Single cell protein. Crit Rev Biotechnol 1983;1:21–57.
[5] Sakarika M, Ganigué R, Rabaey K. Methylotrophs: from C1 compounds to food. Curr Opin Biotechnol 2022;75:102685.
[6] Bachleitner S, Ata Ö, Mattanovich D. The potential of CO2-based production cycles in biotechnology to fight the climate crisis. Nat Commun 2023;14:6987.
[7] Cotton CA, Claassens NJ, Benito-Vaquerizo S, Bar-Even A. Renewable methanol and formate as microbial feedstocks. Curr Opin Biotechnol 2020;62:168–80.
[8] Searchinger TD, Wirsenius S, Beringer T, Dumas P. Assessing the efficiency of changes in land use for mitigating climate change. Nature 2018;564:249–53.
[9] Muhieddine D, Meramo S, Sukumara S. Ranking economic and environmental performance of feedstocks used in bio-based production systems. Curr Res Biotechnol 2025;9:100275.
[10] Kuzman M, Ata Ö, Mattanovich D. Advancing yeast metabolism for a sustainable single carbon bioeconomy. FEMS Yeast Res 2025;25:foaf020.
[11] Mauri A, García, Tejada L, Blank LM. Yeast Midas' touch: recent advances in the valorisation of methanol by yeasts. World J Microbiol Biotechnol 2025;41:422.
[12] Cai P, et al. Methanol biotransformation toward high-level production of fatty acid derivatives by engineering the industrial yeast Pichia pastoris. Proc Natl Acad Sci USA 2022;119:e2201711119.
[13] Bragato N, et al. Revisiting applications of itaconic acid-based polymers obtained by (poly)condensation chemistry. Green Chem 2026;28. https://doi.org/10.1039/d5gc06888f.
[14] Martin GJO, Chan S. Future production of yeast biomass for sustainable proteins: a critical review. Sustain Food Technol 2024;2:1592–609.
[15] Konzock O, Nielsen J. Trends in Biotechnology TRYing to evaluate production costs in microbial biotechnology. Trends Biotechnol 2024;42:1339–47.
[16] Leger D, et al. Photovoltaic-driven microbial protein production can use land and sunlight more efficiently than conventional crops. Proc Natl Acad Sci USA 2021;118:e2015025118.
[17] Krüsemann JL, Rainaldi V, Cotton CAR, Claassens NJ, Lindner SN. The cofactor challenge in synthetic methylotrophy: bioengineering and industrial applications. Curr Opin Biotechnol 2023;82:102953.
[18] Heggeset TMB, Wendisch VF, Vorholt JA, Brautaset T. Methylotrophy in the thermophilic Bacillus methanolicus, basic insights and application for commodity production from methanol. Appl Microbiol Biotechnol 2015;99:535–51.
[19] Ochsner AM, Sonntag F, Buchhaupt M, Schrader J, Vorholt JA. Methylobacterium extorquens: methylotrophy and biotechnological applications. Appl Microbiol Biotechnol 2015;99:517–34.
[20] Yurimoto H, Oku M, Sakai Y. Yeast Methylotrophy: Metabolism, Gene Regulation and Peroxisome Homeostasis. Int J Microbiol 2011;1:101298.
[21] Ozimek P, Veenhuis M, van der Klei IJ. Alcohol oxidase: A complex peroxisomal, oligomeric flavoprotein. FEMS Yeast Res. 2005;5:975–83.
[22] Whitaker WB, Sandoval NR, Bennett RK, Fast AG, Papoutsakis ET. Synthetic methylotrophy: engineering the production of biofuels and chemicals based on the biology of aerobic methanol utilization. Curr Opin Biotechnol 2015;33:165–75.
[23] van der Klei, I.J., Yurimoto, H., Sakai, Y. & Veenhuis, M. The significance of peroxisomes in methanol metabolism in methylotrophic yeast. Biochim Biophys Acta, 1763, 2006, 1453–1462.
[24] Rußmayer H, et al. Systems-level organization of yeast methylotrophic lifestyle. BMC Biol 2015;13:80.

[25] Valli M, et al. A subcellular proteome atlas of the yeast Komagataella phaffii. FEMS Yeast Res 2020;20:foaa001.
[26] Kurtzman CP. A new methanol assimilating yeast, Ogataea parapolymorpha, the ascosporic state of Candida parapolymorpha. Antonie Van Leeuwenhoek 2011;100:455–62.
[27] Manfrão-Netto JHC, Gomes AMV, Parachin NS. Advances in Using Hansenula polymorpha as Chassis for Recombinant Protein Production. Front Bioeng Biotechnol 2019;7:94.
[28] Gellissen G, et al. New yeast expression platforms based on methylotrophic Hansenula polymorpha and Pichia pastoris and on dimorphic Arxula adeninivorans and Yarrowia lipolytica – A comparison. FEMS Yeast Res 2005;5:1079–96.
[29] Mattanovich D, et al. Recombinant Protein Production in Yeasts. In: Lorence A, editor. Recombinant Gene Expression, 824. Humana Press; 2011. p. 329–58.
[30] Zahrl RJ, Peña DA, Mattanovich D, Gasser B. Systems biotechnology for protein production in Pichia pastoris. FEMS Yeast Res 2017;17:fox068.
[31] Bachleitner S, Severinsen M, Lutz G, Mattanovich D. Overexpression of the transcriptional activators Mxr1 and Mit1 enhances lactic acid production on methanol in Komagataella phaffii. Metab Eng 2024;85:133–44.
[32] Severinsen MM, Bachleitner S, Modenese V, Ata Ö, Mattanovich D. Efficient production of itaconic acid from the single-carbon substrate methanol with engineered Komagataella phaffii. Biotechnol Biofuels Bioprod 2024;17:98.
[33] Bachleitner S, Lutz L, Lutz G, Mattanovich D. Bioconversion of the C1 substrate methanol to succinic acid with engineered Komagataella phaffii. Bioresour Technol 2026;453:134603.
[34] Yu W, et al. Methanol biotransformation for the production of biodegradable plastic monomer L-lactate in yeast. Nat Commun 2025;16:10756.
[35] Wefelmeier K, Schmitz S, Kösters BJ, Liebal UW, Blank LM. Methanol bioconversion into C3, C4, and C5 platform chemicals by the yeast Ogataea polymorpha. Microb Cell Fact 2024;23:8.
[36] Wefelmeier K, et al. Engineering the methylotrophic yeast Ogataea polymorpha for lactate production from methanol. Front Bioeng Biotechnol 2023;11:1223726.
[37] Peña DA, Gasser B, Zanghellini J, Steiger MG, Mattanovich D. Metabolic engineering of Pichia pastoris. Metab Eng 2018;50:2–15.
[38] Prielhofer R, et al. GoldenPiCS: A Golden Gate-derived modular cloning system for applied synthetic biology in the yeast Pichia pastoris. BMC Syst Biol 2017;11:123.
[39] Gassler T, Heistinger L, Mattanovich D, Gasser B, Prielhofer R. CRISPR/Cas9-mediated homology-directed genome editing in Pichia pastoris. Methods Mol Biol 2019;1923:211–25.
[40] Tomàs-Gamisans M, Ferrer P, Albiol J. Fine-tuning the P. pastoris iMT1026 genome-scale metabolic model for improved prediction of growth on methanol or glycerol as sole carbon sources. Microb Biotechnol 2018;11:224–37.
[41] Amuel C, Gellissen G, Hollenberg CP, Suckow M. Analysis of heat shock promoters in Hansenula polymorpha: The TPS1 promoter, a novel element for heterologous gene expression. Biotechnol Bioprocess Eng 2000;5:247–52.
[42] Kurylenko OO, et al. Metabolic engineering and classical selection of the methylotrophic thermotolerant yeast Hansenula polymorpha for improvement of high-temperature xylose alcoholic fermentation. Microb Cell Fact 2014;13:122.
[43] Zavec D, Gasser B, Mattanovich D. Characterization of methanol utilization negative Pichia pastoris for secreted protein production: New cultivation strategies for current and future applications. Biotechnol Bioeng 2020;117:1394–405.
[44] Zavec D, et al. Beyond alcohol oxidase: the methylotrophic yeast Komagataella phaffii utilizes methanol also with its native alcohol dehydrogenase Adh2. FEMS Yeast Res 2021;21:foab009.
[45] Claassens NJ, Cotton CAR, Kopljar D, Bar-Even A. Making quantitative sense of electromicrobial production. Nat Catal 2019;2:437–47.
[46] Moritz C, et al. Alcohol dehydrogenase-mediated methanol dissimilation increases carbon efficiency in synthetic autotrophic yeast. bioRxiv 2026. https://doi.org/10.64898/2026.03.09.710585.
[47] Jordà J, De Jesus SS, Peltier S, Ferrer P, Albiol J. Metabolic flux analysis of recombinant Pichia pastoris growing on different glycerol/methanol mixtures by iterative fitting of NMR-derived 13C-labelling data from proteinogenic amino acids. N Biotechnol 2014;31:120–32.
[48] Kok S, De, Kozak BU, Pronk JT, Maris AJA. Van. Energy coupling in Saccharomyces cerevisiae: selected opportunities for metabolic engineering. FEMS Yeast Res 2012;12:387–97.
[49] Dijkhuizen L, Arfman N. Methanol Metab thermotolerant methylotrophic Bacillus Species 1990;87:215–9.
[50] Lin NX, He RZ, Xu Y, Yu XW. Augmented peroxisomal ROS buffering capacity renders oxidative and thermal stress cross-tolerance in yeast. Microb Cell Fact 2021;20:131.
[51] Skryabin KG, et al. Genome sequence and analysis of methylotrophic yeast Hansenula polymorpha DL1. BMC Genom 2013;14:837.
[52] Moritz C, Gassler T, Altvater M. Adaptive Laboratory Evolution of Pichia pastoris by Serial Batch Cultivation. In: Garcia-Ortega X, Glieder A, Kovar K, Rieder L, editors. Pichia pastoris, 2697. Springer Protocols; 2026. p. 373–85.
[53] Mans, R., Daran, J.G. & Pronk, J.T. Under pressure: evolutionary engineering of yeast strains for improved performance in fuels and chemicals production. *Curr. Opin. Biotechnol.* **50**, 2018, 47–56.
[54] Küberl A, et al. High-quality genome sequence of Pichia pastoris CBS7435. J Biotechnol 2011;154:312–20.
[55] Sibirny AA. Yeast peroxisomes: structure, functions and biotechnological opportunities. FEMS Yeast Res 2016;16:4.
[56] Gardner BM, et al. The peroxisomal AAA-ATPase Pex1/Pex6 unfolds substrates by processive threading. Nat Commun 2018;9:135.
[57] Treangen TJ, Salzberg SL. Repetitive DNA and next-generation sequencing: computational challenges and solutions. Nat Rev Genet 2012;13:36–46.
[58] De Schutter K, et al. Genome sequence of the recombinant protein production host Pichia pastoris. Nat Biotechnol 2009;27:561–6.
[59] Nomura M, Nogi Y, Oakes M. Transcription of rDNA in the Yeast Saccharomyces cerevisiae rDNA Structure and Cis-Elements. Madame Curie Bioscience Database. Landes Bioscience; 2003. p. 1–25.
[60] Obayashi BTK. Ribosomal RNA gene repeats, their stability and cellular senescence. Proc Jpn Acad Ser B Phys Biol Sci 2014;90:119–29.
[61] Cabal GG, et al. SAGA interacting factors confine sub-diffusion of transcribed genes to the nuclear envelope. Nature 2006;441:770–3.
[62] Nielsen J. The Power of Yeast. Yeast 2025;42:303–10.
[63] Lee B, Yurimoto H, Sakai Y, Kato N. Physiological role of the glutathione-dependent formaldehyde dehydrogenase in the methylotrophic yeast Candida boidinii. Microbiol (U Kingd) 2002;148:2697–704.
[64] Shen S, Sulter G, Jeffries TW, Cregg JM. A strong nitrogen source-regulated promoter for controlled expression of foreign genes in the yeast Pichia pastoris. Gene 1998;216:93–102.
[65] Yu Y, Yang J, Zhao F, Lin Y, Han S. Comparative transcriptome and metabolome analyses reveal the methanol dissimilation pathway of Pichia pastoris. BMC Genom 2022;23:366.
[66] Berrios J, et al. Role of Dissimilative Pathway of Komagataella phaffii (Pichia pastoris): Formaldehyde Toxicity and Energy Metabolism. Microorganisms 2022;10:1466.
[67] Li K, et al. Improved methanol utilization of Komagataella phaffii by rebuilding metabolic network based on new alcohol-aldehyde transformation system. J Biotechnol 2025;406:60–70.
[68] Zhan C, et al. Reprogramming methanol utilization pathways to convert Saccharomyces cerevisiae to a synthetic methylotroph. Nat Catal 2023;6:435–50.
[69] Guo F, et al. Evolutionary engineering of Saccharomyces cerevisiae: Crafting a synthetic methylotroph via self--reprogramming. Sci Adv 2024;10:eadq3484.
[70] Guo Y, et al. Engineering yeasts to Co-utilize methanol or formate coupled with CO2 fixation. Metab Eng 2024;84:1–12.
[71] Mitic B, et al. The oxygen-tolerant reductive glycine path- way assimilates methanol, formate and CO2 in the yeast Komagataella phaffi. Nat Commun 2023;14:7754.
[72] Kuzman M, Sanvito L, Mitic BM, Ata Ö, Mattanovich D. Rewiring methanol metabolism in Komagataella phaffii through implementation and evolution of a heterologous RuMP cycle. Metab Eng 2026;96:28–38.
[73] Stratton J, Chiruvolu V, Meagher M. High cell-density fermentation. Methods Mol Biol 1998;103:107–20.
[74] Jiménez ER, Sánchez K, Roca H, Delgado JM. Different methanol feeding strategies to recombinant Pichia pastoris cultures producing high level of dextranase. Biotechnol Tech 1997;11:461–6.
[75] Cos O, Ramón R, Montesinos JL, Valero F. Operational strategies, monitoring and control of heterologous protein production in the methylotrophic yeast Pichia pastoris under different promoters: A review. Microb Cell Fact 2006;5:17. https://doi.org/10.1186/1475-2859-5-17.
[76] Koch C, Neumann P, Valerius O, Feussner I, Ficner R. Crystal Structure of Alcohol Oxidase from Pichia pastoris. PLoS One 2016;11:e0149846.
[77] Shleev SV, et al. Purification and Characterization of Alcohol Oxidase from a Genetically Constructed Over producing Strain of the Methylotrophic Yeast Hansenula polymorpha. Biochemistry (Mosc) 2006;71:245–50.
[78] Krüsemann JL, Rainaldi V, Cotton CA, Claassens NJ, Lindner SN. The cofactor challenge in synthetic methylotrophy: bioengineering and industrial applications. Curr Opin Biotechnol 2023;82:102953.
[79] Zavec D. Engineering Pichia pastoris for improved methanol utilization Dissertation. BOKU University; 2019.
[80] Van Dijken LP, Otto R, Harder W. Growth of Hansenula polymorpha in a methanol-limited chemostat - Physiological responses due to the involvement of methanol oxidase as a key enzyme in methanol metabolism. Arch Microbiol 1976;111:137–44.
[81] Wendisch VF, Kosec G, Heux S, Brautaset T. Aerobic Utilization of Methanol for Microbial Growth and Production. Adv Biochem Eng/Biotechnol 2022;180:169–212.
[82] Gassler T, Baumschabl M, Sallaberger J, Egermeier M, Mattanovich D. Adaptive laboratory evolution and reverse engineering enhances autotrophic growth in Pichia pastoris. Metab Eng 2022;69:112–21.
[83] Akşit A, van der Klei IJ. Yeast peroxisomes: How are they formed and how do they grow? Int J Biochem Cell Biol 2018;105:24–34.
[84] Hümmler LM, Hristov S, Hille L, Noor E, Lindner SN. Resolving misconceptions and constraints in growth- coupled bioproduction. Curr Opin Biotechnol 2026;96:103388.
[85] Gassler T, et al. The industrial yeast Pichia pastoris is converted from a heterotroph into an autotroph capable of growth on CO2. Nat Biotechnol 2020;38:210–6.
[86] Valli M, et al. Curation of the genome annotation of Pichia pastoris (Komagataella phaffii) CBS7435 from gene level to protein function. FEMS Yeast Res 2016;16:fow051.